A fully interior penalty discontinuous Galerkin method for variable density groundwater flow problems

Ali Raeisi Isa-Abadi, Vincent Fontaine, Hamid-Reza Ghafouri, Anis Younes, Marwan Fahs

Version of Record: https://www.sciencedirect.com/science/article/pii/S0045793020303145
Manuscript_85f33e657c3dc979c6f3939dd7bcd57f

A fully interior penalty discontinuous Galerkin method for variable density groundwater flow problems

Ali Raeisi Isa-Abadi[a], Vincent Fontaine[b], Hamid-Reza Ghafouri[c], Anis Younes[d], Marwan Fahs[d,*]

[a]*Department of Water Engineering, Shahrekord University, Shahrekord, Iran*
[b]*Department of Building and Environmental Sciences,University of Réunion, Le Tampon, France*
[c]*Department of Civil Engineering, Shahid Chamran University of Ahvaz, Ahvaz, Iran*
[d]*Université de Strasbourg, CNRS, ENGEES, LHYGES UMR 7517, F-67000 Strasbourg, France*

Abstract

Discontinuous Galerkin (DG) methods due to their robustness properties, e.g. local conservation, low numerical dispersion, and well-capturing strong shocks and physical discontinuities, are well-suited for the simulation of Variable Density Flow (VDF) in porous media. This paper aims at introducing, in a unified format, the general class of Interior Penalty DG (IPDG) methods to solve the VDF equations. A combination of symmetric, non-symmetric and incomplete IPDG methods is used to discretize both head and concentration variables. Compatibility analysis is performed to prevent the loss of accuracy of the IPDG methods in simulations of coupled flow and transport equations. An accurate technique is used for time integration, based on a non-iterative procedure and adaptive time stepping with embedded error control. Several benchmarks are investigated to validate the proposed DG scheme and to examine its performance in simulating VDF problems. The new DG scheme reproduces better the experimental data than the conventional SEAWAT model. Its results are in excellent agreement with a recent semi-analytical solution of the Henry problem, dealing with seawater intrusion under convection-dominating conditions. The performance of the DG scheme is examined by simulating the challenging problem of natural convection in porous enclosure. The method is compared against a finite element solution obtained with COMSOL multi-physics. The numerical experiments indicate clearly that high-order DG method is much more appropriate than standard conforming Galerkin method in simulating VDF problems while at the same time, guaranteeing a better precision and high-fidelity solutions. The proposed numerical method can be extended to 3D problems.

Keywords: Variable density flow, Compatible algorithms, Advanced model, seawater intrusion, Natural convection in porous enclosures

1. Introduction

Numerical modeling of variable density flow (VDF) has an irreplaceable role in predicting the groundwater behaviour in several applications such as seawater intrusion, saltwater upconing, geothermal systems, underground nuclear waste disposal, and carbon sequestration. In such situations, a coupled nonlinear system of flow and transport equations is commonly used to describe the physical processes. Simulation

*Corresponding author
Email address: fahs@unistra.fr (Marwan Fahs)

of VDF problems requires accurate methods as numerical artifacts can affect the results, especially in unstable cases. This is also why benchmarking VDF numerical models is a common issue which has been widely discussed in the literature [30, 65, 73, 74, 77, 84]. Clearly, in a numerical simulation, the level of the solution accuracy profoundly depends on the applied numerical scheme.

In the literature, several studies investigated the different aspects of VDF numerical modelling. For instance, Mazzia and Putti [56] validated the formulations resulting from the combination of two sets of dependent variables, i.e. head/concentration and pressure/mass-fraction, and concluded that the latter one is more accurate especially in long simulation periods. Comparison of conservative and non-conservative formulations [62] and validity of Oberbeck-Boussinesq based formulation were also explored [36, 47, 49]. Younes et al. [92] studied the efficiency of high-order time integration schemes to solve the partial differential equations of the VDF model. Different time-stepping techniques have been also investigated in Hirthe and Graf [41], Younes and Ackerer [89]. Consistent velocity approximation is one of the numerical challenges addressed by Albets-Chico and Kassinos [5], Diersch and Kolditz [20], Frolkovič [32], Herbert et al. [40], Voss and Souza [85]. Another common challenge that the authors have encountered is the solution of the coupled nonlinear systems obtained from numerical discretization. For example, Putti and Paniconi [66] presented a partial Newton method in order to reduce the size of matrix systems equal to that of Picard. A new coupling procedure was also proposed by Ackerer [2] to improve the rate of convergence in Picard method. However, one of the most crucial questions for the numerical solution of the VDF model is the discretization of the spatial derivatives. Numerous studies have been devoted to the various spatial discretization methods such as the finite difference method [15, 37], the finite element method [19, 45, 72], the finite volume method [33, 38], and the method of characteristics [63, 64]. However, using the conventional discretization methods (especially standard Galerkin finite element and finite difference methods) for the transport equation leads to numerical dispersion [57, 86], and using nonconservative methods for the flow equation in a coupled system can result in erroneous solutions [21].

DG methods were firstly introduced in the middle of the seventies for the numerical approximation of hyperbolic problems, and independently, in the context of elliptic and parabolic problems [see e.g., 8, 9, 14]. For diffusion problems, Arnold [7] introduced a primal DG method inspired by the original work of Nitsche (1971) using Interior Penalty (IP) technique to weakly enforce some regularity requirements of the solution across the skeleton of the mesh. This derivation yields to the Symmetric Interior Penalty (SIP) method and constitutes a milestone in the development of primal DG methods. In the late 1990s, numerous variations of the SIP method have been proposed and studied in the literature. For instance, Oden et al. [61] introduced the Oden–Babuška–Baumann (OBB) method for pure diffusion problems and then extended it to convection-diffusion processes [11]. Compared to SIP, the differences lie in the use of consistency and penalty terms at interfaces that are now skew-symmetric and null, respectively. Alternatively, penalty terms have been added to the OBB formulation leading to the Non-symmetric Interior Penalty (NIP) method analyzed by Rivière et al. [70]. Finally, we mention the Incomplete Interior Penalty (IIP) method

as introduced first by Dawson et al. [16]. Thus, symmetric, non-symmetric and incomplete interior Penalty methods are the three most famous variations of the primal DG method, and they have been judiciously combined to solve efficiently coupled single-phase flow and reactive transport problems [see e.g., 16, 80, and the references therein]. The DG methods are numerically stable even for high Péclet numbers, able to capture physical discontinuities well and to handle nonconforming and unstructured meshes [1, 31]. They are locally adaptive in mesh and polynomial degrees and are well suited for efficient parallel implementations [see e.g. 14, 57, 79, and references therein].

Since its introduction, and due to their advantages, DG methods have benefited from intensive research and development, and they have been applied to a variety of physical issues and situations. In the context of porous media, the DG method has been used to discretize the hyperbolic terms of the governing equations in applications involving contaminant transfer in aquifers [88], two phase flow nonfractured domains [27, 34, 51, 94], two phase flow in fractured domains [42, 43, 58, 59, 93] and diffusion and natural convection in fractured domains [44]. In this context, the combination of DG method and mixed finite element (MFE) method has received particular attention. The former has been used to discretize the convective term of the transport equation while the later has been used for flow. Sun et al. [78] used this combination with a cut-off operator in DG method to make the method converge. Li and Riviere [55] developed a discretization method based on the combination of MFE-DG without any slope limiter into heterogeneous media which uses a high-order Runge-Kutta approximation for time.

The DG method has been also used to entirely solve the flow or transport (both hyperbolic and parabolic terms) equations in porous media. Li and Riviere [54] used a weighted version of high-order IPDG methods for simulation of miscible displacement problems. Besides, Rivière and Wheeler [69] described a full DG method with slope limiter for miscible displacement. For a coupled system of flow and reactive transport, a fully primal DG using a cut-off operator was developed by Sun and Wheeler [79]. Full primal DG method was used to simulate two-phase flow in Arbogast et al. [6], Bastian [10], Epshteyn and Rivière [23, 24, 25], Ern et al. [26], Jamei et al. [46], Kou and Sun [50], Mozolevski and Schuh [60]. The three primal DG methods, namely IIP, SIP, and NIP methods were discussed in these works. Different DG methods have been also used to investigate variably-saturated flow expressed by Richards equation [17, 22, 52, 53] and reactive transport in porous media [79–83, 87].

This brief review shows an increasing interest in the development and utilization of the DG methods in several applications related to flow and mass transfer in fractured/unfractured porous media. The review paper by Miller et al. [57] estimated that, with the advancement of computing technology, DG methods have great potential to be foundational technique for future simulators of multi-physical processes in porous media and more generally for future solvers of physical partial differential equations. The dynamic adaptivity properties and localized nature of DG methods, especially, are well-adapted for many VDF situations where the dense physics/high spatial gradients occur only in a small space may vary continuously over time. Thereby, a comparable memory and processing time can be saved. However, despite their

advantages, wide range of applications, increasing popularity and promising results, applications of DG methods in VDF are limited and performance of these methods in such a configuration has been never evaluated. For VDF, the DG methods have been only used for discretizing the convective terms of the transport equation and has been coupled with other methods (mainly MFE) for discretizing the flow and parabolic term of the transport equation [3, 4, 13, 92].

DG methods have never been used to solve the full VDF model while this could be very advantageous. In a full DG model, one can efficiently solve pure diffusion, pure advection or any mixed situation with one and only one mathematical formalism, no splitting operator techniques, no need to introduce different variables for the diffusive and convective parts, and solution procedure can be efficiently accelerated using parallel computing. This avoids splitting errors and allows for treating mixed boundary conditions in accurate manner. Thus, the main aim of the present work is to show how DG methods can be used to solve the full VDF model and to evaluate the performance and benefits of this class of methods in simulating VDF problems. We develop a unified and coherent format of the general class of IPDG. We test symmetric, non-symmetric and incomplete IPDG methods to discretize flow and transport variables (pressure head and concentration). Flow and transport equations are solved sequentially. We implement an efficient scheme for time integration based on adaptive time stepping with error control. The new developed numerical scheme is validated against experimental data and semi-analytical solutions for problems involving VDF driven by salinity gradients. A highly convective thermal-driven case is considered to evaluate the performance of the developed DG scheme, by comparing it against standard finite element solution obtained with COMSOL Multiphysics.

The paper is organized as follows: In section 2, we describe the governing equations. Section 3 is devoted to the discretization of the governing equations using the IPDG method and to the numerical scheme implemented to solve the discretized equations. Section 4 aims at validating and verifying the new developed scheme by comparison against semi-analytical solutions (Henry and thermal porous-cavity problems) and experimental data. To highlight the performance of the developed DG scheme, a convergence analysis is presented in section 4. Finally, we end in section 5 with general conclusions.

2. Governing equations

The governing equations of variable density groundwater flow and solute transport are described following [12, 45, 49]. The set of partial differential equations include (i) the generalized Darcy' law, (ii) continuity equations of fluid and solute mass, and (iii) state equations for the bulk fluid density and/or viscosity. We will propose an equivalent compact formulation of both original problems based on the introduction of suitable variables. In the rest of the paper, we assume that previous coupled physical processes are given in a bounded domain $\Omega \subset \mathbb{R}^2$ with a Lipschitz boundary $\partial\Omega$, and in time interval $[0, T]$, with $T > 0$.

2.1. Variable density flow equation

The generalized Darcy' law can be written in term of the reference head variable $\varphi = p/(\rho_0 g) + z$ where p corresponds to the dynamic pressure $[ML^{-1}T^{-2}]$, ρ_0 the reference fluid density $[ML^{-3}]$, z the vertical elevation above some datum level $[L]$, and g the gravity acceleration $[LT^{-2}]$. Namely,

$$\mathbf{q} = -\mathbf{K}\left(\nabla\varphi + \frac{\rho - \rho_0}{\rho_0}\nabla z\right) \qquad \text{in} \quad \Omega \times (0, T], \tag{1}$$

where $\mathbf{q}$ denotes the Darcy's velocity $[LT^{-1}]$ and ρ is the fluid density $[ML^{-3}]$. Here, $\mathbf{K} = \frac{\rho_0 g \mathbf{k}}{\mu}$ is defined as hydraulic conductivity where $\mathbf{k}$ is the permeability tensor of the porous material $[L^2]$, and μ the bulk fluid viscosity $[ML^{-1}T^{-1}]$. Following Huyakorn et al. [45], the time-dependent mass balance equation of the fluid in a porous medium is given by:

$$\rho s \partial_t \varphi + \phi \partial_c \rho \partial_t c + \nabla\cdot(\rho\mathbf{q}) = 0, \quad \text{in} \quad \Omega \times (0, T], \tag{2}$$

where s is the specific storativity of the porous medium related to head change $[L^{-1}]$, c the solute mass fraction $[-]$, ϕ the kinematic porosity $[-]$, and ∂_x the partial derivative operator with respect to the x-variable. The boundary $\partial\Omega$ is divided into a Dirichlet part, $\partial\Omega_D$, and a Neumann part, $\partial\Omega_N$, such that $\partial\Omega_D \cup \partial\Omega_N = \partial\Omega$ and $\partial\Omega_D \cap \partial\Omega_N = \emptyset$. Thus, the boundary and initial conditions for the flow process are given by:

$$\varphi = \varphi_D, \quad \text{on} \quad \partial\Omega_D \times (0, T], \tag{3a}$$

$$\rho\mathbf{q}\cdot\mathbf{n} = q_N, \quad \text{on} \quad \partial\Omega_N \times (0, T], \tag{3b}$$

$$\varphi(\cdot, 0) = \varphi^0, \quad \text{in} \quad \Omega \times \{0\}, \tag{3c}$$

where $\mathbf{n}$ is the outward unit normal vector on $\partial\Omega$, φ_D and q_N are prescribed functions on $\partial\Omega_D$ and $\partial\Omega_N$, respectively.

2.2. Solute transport equation

The solute transport process is governed by a time-dependent advection-dispersion equation,

$$\partial_t(\phi\rho c) + \nabla\cdot(\rho\mathbf{q}c - \rho\mathbf{D}\nabla c) = 0, \quad \text{in} \quad \Omega \times (0, T]. \tag{4}$$

Here $\mathbf{D}$ corresponds to the hydrodynamic dispersion tensor $[L^2T^{-1}]$ given by,

$$\mathbf{D} = (\alpha_T|\mathbf{q}| + \phi D_m)\,\mathbf{I} + (\alpha_L - \alpha_T)\,\frac{\mathbf{q}\otimes\mathbf{q}}{|\mathbf{q}|}, \tag{5}$$

where $\otimes$ denotes the dyadic product, $|\cdot|$ the Euclidean norm, D_m the molecular diffusion coefficient $[L^2T^{-1}]$, $\mathbf{I}$ the identity tensor, and α_L and α_T the longitudinal and transverse dispersivity, respectively $[L]$. The domain boundary is now splitted into the inflow part, $\partial\Omega_{\text{in}} := \{\mathbf{x} \in \partial\Omega : \mathbf{q}\cdot\mathbf{n} < 0\}$, and the outflow part,

$\partial\Omega_{\text{out}} := \partial\Omega \setminus \partial\Omega_{\text{in}}$, such that $\partial\Omega_{\text{in}} \cup \partial\Omega_{\text{out}} = \partial\Omega$ and $\partial\Omega_{\text{in}} \cap \partial\Omega_{\text{out}} = \emptyset$. Thus, the boundary and initial conditions for the solute transport process are given by:

$$(\rho c\mathbf{q} - \rho\mathbf{D}\nabla c) \cdot \mathbf{n} = \rho_{\text{in}} c_{\text{in}} \mathbf{q} \cdot \mathbf{n}, \quad \text{on} \quad \partial\Omega_{\text{in}} \times (0, T], \tag{6a}$$

$$-\mathbf{D}\nabla c \cdot \mathbf{n} = 0, \quad \text{on} \quad \partial\Omega_{\text{out}} \times (0, T], \tag{6b}$$

$$c\,(\cdot, 0) = c^0, \quad \text{in} \quad \Omega \times \{0\}, \tag{6c}$$

where ρ_{in} and c_{in} are the specified inflow density and mass fraction at the inflow boundary $\partial\Omega_{\text{in}}$, respectively.

2.3. State equation for the bulk fluid density

The state equations represent fundamental thermodynamic relationships reflecting some properties and physical characteristics of a fluid using state variables. In practice, the mathematical dependencies of the bulk fluid density and viscosity quantities are usually derived by using a total derivative representation with respect to the set of state variables. Here, we assume that the bulk fluid density and viscosity depend only on the mass fraction variable, i.e., $\rho = \rho(c)$ and $\mu = \mu(c)$, on the whole domain. We consider the simplest linearized model for the density :

$$\rho = \rho_0 \left(1 + \beta_0 c\right), \quad \text{in} \quad \Omega \times (0, T], \tag{7}$$

where $\beta_0 = \rho_0^{-1} \partial_c \rho$ corresponds to the expansivity coefficient resulting from a change of the solute mass fraction $[-]$. Different mathematical models of state equations have been proposed in the literature, including the thermal effect and based on a polynomial expansion of the state variables. The viscosity is considered as constant in the numerical simulations developed in this work, but the developed DG model can handle variable viscosity.

2.4. Mathematical model

In this section, we propose to rewrite the set of partial differential equations governing variable-density flow with the corresponding initial and boundary conditions in a compact form. To this aim, we introduce suitable variables for the description of each of both processes. Thus, we use the following notations:

$$\text{(Flow)} \quad s^* = \rho s, \quad \beta_0^* = \rho_0 \phi \beta_0, \quad \mathbf{q}^* = \rho\mathbf{q} \quad \text{and} \quad \mathbf{K}^* = \rho\mathbf{K}, \tag{8a}$$

$$\text{(Transport)} \quad \phi^* = \rho\phi, \quad \mathbf{D}^* = \rho\mathbf{D} \quad \text{and} \quad c_{\text{in}}^* = \frac{\rho_{\text{in}} c_{\text{in}}}{\rho}. \tag{8b}$$

Respecting the previous notations, the flow problem is now described by the simplified set of equations:

$$s^* \partial_t \varphi + \beta_0^* \partial_t c + \nabla \cdot \mathbf{q}^* = 0, \quad \text{in} \quad \Omega \times (0, T], \tag{9a}$$

$$\mathbf{q}^* = -\mathbf{K}^* \left(\nabla\varphi + \beta_0 c \nabla z\right), \quad \text{in} \quad \Omega \times (0, T], \tag{9b}$$

where the initial and Dirichlet boundary conditions (3a)-(3c) remain unchanged, and the Neumann condition (3b) becomes:

$$\mathbf{q}^* \cdot \mathbf{n} = q_N, \quad \text{on} \quad \partial\Omega_N \times (0, T]. \tag{10a}$$

The time-dependent advection-dispersion equation now can be written as follows:

$$\gamma\partial_t(c) + \nabla\cdot(\mathbf{q}^* c - \mathbf{D}^*\nabla c) = 0, \quad \text{in} \quad \Omega\times(0,T], \tag{11}$$

where $\gamma(c) = \phi^* + \beta_0^* c$, with the following boundary conditions

$$(c\mathbf{q}^* - \mathbf{D}^*\nabla c)\cdot\mathbf{n} = c_{\text{in}}^*\mathbf{q}^*\cdot\mathbf{n}, \quad \text{on} \quad \partial\Omega_{\text{in}}\times(0,T], \tag{12a}$$

$$-\mathbf{D}^*\nabla c\cdot\mathbf{n} = 0, \quad \text{on} \quad \partial\Omega_{\text{out}}\times(0,T]. \tag{12b}$$

Let us underline that the initial condition (6c) remains unchanged as well as the definitions of inflow $\partial\Omega_{\text{in}}$ and outflow $\partial\Omega_{\text{out}}$ boundary parts since $\rho > 0$.

3. Interior penalty discontinuous Galerkin methods

The class of Interior Penalty discontinuous Galerkin (IPDG) methods is now derived to solve the coupled non-linear system of partial differential equations. Precisely, we consider the Incomplete Interior Penalty (IIP), the Symmetric Interior Penalty (SIP) and the Non-symmetric Interior Penalty (NIP) variants for each physical process leading to nine possible combinations schemes. The main difference between these three IP variants lies in the symmetrization term used in the discrete bilinear form [68]. Before establishing the weak formulations, let us introduce some conventional notations that will be used throughout the remainder of the paper.

3.1. Some notations

We denote by $0 = t_0 < t_1 < t_2 < \ldots < t_N = T$ a non-uniform partition of the simulation time interval $(0,T]$. Let $\mathcal{E}_h = \{E_i\}_{N_h}$ be a partition of the domain $\bar{\Omega}$ into a set of quasi-uniform conforming triangular elements, E denotes an element with the boundary ∂E and area $|E|$, and $h = \max_{E\in\mathcal{E}_h} h_E$ where $h_E = \text{diam}\,(E)$. Let N_{loc}^H and N_{loc}^c be the number of degrees of freedom (DOFs) per element for head and mass fraction, respectively. Let $\mathcal{F}_h$ be the set of all edges comprising interior and boundary edges such that $\mathcal{F}_h = \mathcal{F}_h^I \cup \mathcal{F}_h^B$. Let Γ be an interior edge $\Gamma \in \mathcal{F}_h^I$ with size $|\Gamma|$, then there exist two adjacent elements $E_\Gamma^\pm$ such that $\Gamma = \partial E_\Gamma^- \cap \partial E_\Gamma^+$. Further, we denote $\mathbf{n}_\Gamma^\pm$ the unit normal vector on Γ pointing exterior to $E_\Gamma^\pm$, respectively (see e.g., Fig. 1), and $\mathbf{n}_\Gamma$ is coincident with $\mathbf{n}_\Gamma^+$. Let Γ be a boundary edge $\Gamma \in \mathcal{F}_h^B$, then there exist an element $E \in \mathcal{E}_h$ such that $\Gamma = \partial E \cap \partial\Omega$. We define the set of Dirichlet, Neumann, inflow and outflow edges such that $\mathcal{F}_h^B = \mathcal{F}_h^D \cup \mathcal{F}_h^N = \mathcal{F}_h^{\text{in}} \cup \mathcal{F}_h^{\text{out}}$. For clarity purposes, we denote by $\mathcal{F}_h^0 := \mathcal{F}_h^I \cup \mathcal{F}_h^D$ for the flow problem, and by $\mathcal{F}_h^+ := \mathcal{F}_h^I \cup \mathcal{F}_h^{\text{out}}$ for the solute transport problem. The DG method is based on the use of discontinuous approximations of discrete variables. To this aim, let us introduce the broken polynomial space $\mathcal{V}_h^p$ which is a finite dimensional space of discontinuous piecewise polynomial functions belonging to the broken Sobolev space $\mathcal{H}^s(\mathcal{E}_h)$ with $s \geq 1$,

$$\mathcal{V}_h^p := \left\{ v \in L^2(\Omega) : v|_E \in \mathbb{P}_p(E) \quad \forall E \in \mathcal{E}_h \right\},$$

where $\mathbb{P}_p(E)$ corresponds to the space of all polynomials of total degree $\leq p$ on E. Let $\psi_\Gamma^\pm$ be the traces of function ψ on the edge Γ between $E_\Gamma^\pm$. Therefore, p_φ and p_c are taken to be the total degrees of discontinuous polynomials for approximating reference head and mass fraction, respectively. The jump and

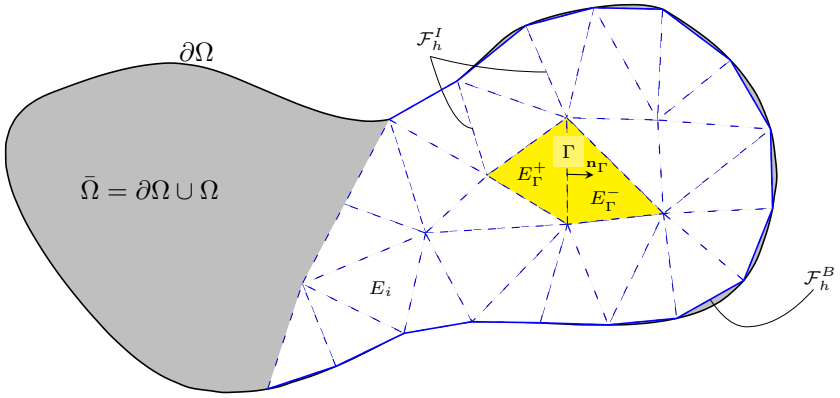

Fig. 1. Schematic discretization of $\bar{\Omega}$ and representation of elements, interior and boundary edges

average of ψ on Γ can be now defined on the skeleton $\mathcal{F}_h$ as follows,

$$[\![\psi]\!] := \begin{cases} \psi_\Gamma^- \mathbf{n}_\Gamma^- + \psi_\Gamma^+ \mathbf{n}_\Gamma^+, & \text{if} \quad \Gamma \in \mathcal{F}_h^I, \\ \psi \mathbf{n}, & \text{if} \quad \Gamma \in \mathcal{F}_h^B, \end{cases} \tag{13a}$$

$$\{\!\{\psi\}\!\} := \begin{cases} \left(\psi_\Gamma^- + \psi_\Gamma^+\right)/2, & \text{if} \quad \Gamma \in \mathcal{F}_h^I, \\ \psi, & \text{if} \quad \Gamma \in \mathcal{F}_h^B. \end{cases} \tag{13b}$$

Let us precise that previous definitions of trace operators can be easily extended to any vector-valued functions ψ in the same way. For all $\boldsymbol{x} := (x_1, \ldots, x_p) \in \mathbb{R}^p$ with $p \geq 1$, we define the uniform norm of $\boldsymbol{x}$ by $\|\boldsymbol{x}\|_\infty := \max_{1 \leq i \leq p} |x_i|$.

3.2. Spatial discretization of the flow process

The IPDG weak formulations for flow and transport are derived by multiplying the corresponding governing equation by appropriate test functions, integrating by parts over an element $E \in \mathcal{E}_h$ (via the Green theorem), summing-up over all elements of the partition, and finally by imposing initial and boundary conditions. By performing the afore-mentioned operations on the flow problem (9), the weak form (in continuous time) is achieved and consists to seek, for any compatible $c_h(\cdot, t) \in \mathcal{V}_h^{p_c}$, the discrete variable $\varphi_h(\cdot, t) \in \mathcal{V}_h^{p_\varphi}$ such that,

$$(s^* \partial_t \varphi_h, v_h)_{\mathcal{E}_h} + (\beta_0^* \partial_t c_h, v_h)_{\mathcal{E}_h} + a_h^{(\epsilon_f)}(\varphi_h, v_h; c_h) = l_f^{(\epsilon_f)}(v_h; c_h) \qquad \forall v_h \in \mathcal{V}_h^{p_\varphi}, \tag{14}$$

where $\epsilon_f \in \{0, \pm 1\}$ is a symmetrization parameter, and the discrete operators $a_h^{(\epsilon_f)}$ and $l_f^{(\epsilon_f)}$ are given by:

$$\begin{aligned} a_h^{(\epsilon_f)}(\varphi_h, v_h; c_h) = &(\mathbf{K}^*(c_h)\nabla\varphi_h, \nabla v_h)_{\mathcal{E}_h} - \langle \{\!\{\mathbf{K}^*(c_h)\nabla\varphi_h\}\!\}, [\![v_h]\!] \rangle_{\mathcal{F}_h^0} - \epsilon_f \langle \{\!\{\mathbf{K}^*(c_h)\nabla v_h\}\!\}, [\![\varphi_h]\!] \rangle_{\mathcal{F}_h^0} + \\ &\langle \sigma_\Gamma^f [\![\varphi_h]\!], [\![v_h]\!] \rangle_{\mathcal{F}_h^0}, \end{aligned} \tag{15}$$

$$l_f^{(\epsilon_f)}(v_h;c_h) = -(\mathbf{K}^*(c_h)\beta_0 c_h\nabla z,\nabla v_h)_{\mathcal{E}_h} + \langle\{\!\{\mathbf{K}^*(c_h)\beta_0 c_h\nabla z\}\!\},[\![v_h]\!]\rangle_{\mathcal{F}_h^0} - \epsilon_f\langle\mathbf{K}^*(c_h)\nabla v_h\cdot\mathbf{n}_\Gamma,\varphi_D\rangle_{\mathcal{F}_h^D} + \langle\sigma_\Gamma^f\varphi_D,v_h\rangle_{\mathcal{F}_h^D} - \langle q_N,v_h\rangle_{\mathcal{F}_h^N}. \tag{16}$$

The second, third and fourth terms on the right-hand side of (15) are respectively called *consistency*, *symmetry* and *penalty* terms. The role of the parameter ϵ_f consists of regulating the symmetry term impact inside the bilinear form. Here, σ_Γ^f corresponds to the penalty parameter on Γ, and it is defined on the mesh skeleton as follows:

$$\sigma_\Gamma^f = \begin{cases} \dfrac{2\tau_\Gamma^-\tau_\Gamma^+}{\tau_\Gamma^- + \tau_\Gamma^+} & \text{if} \quad \Gamma\in\mathcal{F}_h^I \\ \tau_{E,\Gamma} & \text{if} \quad \Gamma\in\mathcal{F}_h^D \end{cases} \tag{17}$$

where $\tau_\Gamma^\pm = \tau_{E^\pm,\Gamma}$ denotes the transmissibility coefficient on $\Gamma = \partial E^-\cap\partial E^+$. For all $E\in\mathcal{E}_h$, and for any $\Gamma\in\partial E$, this parameter is given by,

$$\tau_{E,\Gamma} = \sigma_0^f\frac{|\Gamma|}{|E|}(p_\varphi+1)(p_\varphi+2)\kappa_{E,\Gamma}, \tag{18}$$

where $\kappa_{E,\Gamma} = \mathbf{n}_\Gamma\mathbf{K}_E^*\mathbf{n}_\Gamma$ represents the normal diffusivity on Γ and $\sigma_0^f\geq 0$ is a user-dependent parameter. The unified DG formalism of the variable density flow problem (14) includes the Incomplete Interior Penalty (IIP), the Symmetric Interior Penalty (SIP), the Non-symmetric Interior Penalty (NIP), and the Oden–Babuška–Baumann (OBB) methods. All these variants are deduced by choosing precisely both parameters ϵ_f and σ_0^f: IIP ($\epsilon_f = 0$ and $\sigma_0^f > 0$), SIP ($\epsilon_f = 1$ and $\sigma_0^f > 0$), NIP ($\epsilon_f = -1$ and $\sigma_0^f > 0$), and OBB ($\epsilon_f = -1$ and $\sigma_0^f = 0$). Regardless of the choice of IP methods, it is a fundamental aspect at this stage to reconstruct the Darcy's velocity field $\mathbf{q}^*$. To this aim, we shall use the favourable local conservation properties associated with IPDG methods. Let us denotes by $\tilde{\mathbf{q}}_h^*$ the discrete approximation of the velocity field $\mathbf{q}^*$ on the partition $\mathcal{E}_h$. Two description levels are used to approximate $\mathbf{q}^*$ (i) at the element-level E of the mesh $\mathcal{E}_h$, and (ii) at the edge-level Γ of the mesh skeleton $\mathcal{F}_h$.

$$\tilde{\mathbf{q}}_h^* = \begin{cases} \mathbf{q}_h^*, & \text{for all} \quad E\in\mathcal{E}_h, \\ \hat{\mathbf{q}}_h^* & \text{for all} \quad \Gamma\in\mathcal{F}_h, \end{cases} \tag{19}$$

where $\mathbf{q}_h^* = -\mathbf{K}^*(c_h)\left(\nabla\varphi_h + \beta_0 c_h\nabla z\right)$ and the numerical flux $\hat{\mathbf{q}}_h^*$ is defined as follow:

$$\hat{\mathbf{q}}_h^* = \begin{cases} \{\!\{\mathbf{q}_h^*\}\!\} + \sigma_\Gamma^f[\![\varphi_h]\!], & \text{if} \quad \Gamma\in\mathcal{F}_h^I \\ \mathbf{q}_h^* + \sigma_\Gamma^f(\varphi_h-\varphi_D)\mathbf{n}_\Gamma, & \text{if} \quad \Gamma\in\mathcal{F}_h^D \\ q_N\mathbf{n}_\Gamma, & \text{if} \quad \Gamma\in\mathcal{F}_h^N \end{cases} \tag{20}$$

3.3. Spatial discretization of the transport process

This section is devoted to the presentation of the IPDG discretization of the transport equation respecting the imposed boundary conditions. We use a similar approach to the previous section to handle the

dispersive part that we combine with a traditional upwind-strategy to control the advective part. Thus, the spatial discretization of the transport problem (in continuous time) consists to seek, for any reconstructed $\tilde{\mathbf{q}}_h^*(\cdot,t)$, the discrete variable $c_h(\cdot,t) \in \mathcal{V}_h^{p_c}$ such that,

$$(\gamma \partial_t c_h, w_h)_{\mathcal{E}_h} + b_h^{(\epsilon_t)}(c_h, w_h; \tilde{\mathbf{q}}_h^*) = l_t^{(\epsilon_t)}(w_h; \tilde{\mathbf{q}}_h^*), \qquad \forall w_h \in \mathcal{V}_h^{p_c}, \tag{21}$$

where $\epsilon_t \in \{0, \pm 1\}$, the discrete bilinear form $b_h^{(\epsilon_t)}$ is given by,

$$\begin{aligned} b_h^{(\epsilon_t)}(c_h, w_h; \tilde{\mathbf{q}}_h^*) = &(\mathbf{D}^*(\mathbf{q}_h^*)\nabla c_h - c_h \mathbf{q}_h^*, \nabla w_h)_{\mathcal{E}_h} + \langle \hat{\mathbf{q}}_h^* \{\!\{c_h\}\!\}, [\![w_h]\!] \rangle_{\mathcal{F}_h^+} - \langle \{\!\{\mathbf{D}^*(\hat{\mathbf{q}}_h^*)\nabla c_h\}\!\}, [\![w_h]\!] \rangle_{\mathcal{F}_h^I} \\ &- \epsilon_t \langle \{\!\{\mathbf{D}^*(\hat{\mathbf{q}}_h^*)\nabla w_h\}\!\}, [\![c_h]\!] \rangle_{\mathcal{F}_h^I} + \langle \sigma_\Gamma^t [\![c_h]\!], [\![w_h]\!] \rangle_{\mathcal{F}_h^I}, \end{aligned} \tag{22a}$$

and the linear form $l_t^{(\epsilon_t)}$ by,

$$l_t^{(\epsilon_t)}(w_h; \tilde{\mathbf{q}}_h^*) = -\langle (\hat{\mathbf{q}}_h^* \cdot \mathbf{n}_\Gamma) c_{\text{in}}, w_h \rangle_{\mathcal{F}_h^{\text{in}}}. \tag{22b}$$

Here, $\sigma_\Gamma^t \geq 0$ corresponds to the penalty parameter for the advective-dispersive problem and we assume that it can decomposed into a dispersive and advective parts,

$$\sigma_\Gamma^t = \frac{2\tau_\Gamma^- \tau_\Gamma^+}{\tau_\Gamma^- + \tau_\Gamma^+} + \frac{1}{2}|\hat{\mathbf{q}}_h^* \cdot \mathbf{n}_\Gamma|, \qquad \forall \Gamma \in \mathcal{F}_h^I, \tag{23}$$

where the parameters $\tau_\Gamma^\pm = \tau_{E^\pm,\Gamma}$ are now derived using the hydrodynamic dispersion tensor $\mathbf{D}^*$ and the polynomial order p_c of the discrete variable c_h. For all $E \in \mathcal{E}_h$, and for any $\Gamma \in \partial E$, it is given by,

$$\tau_{E,\Gamma} = \sigma_0^t \frac{|\Gamma|}{|E|}(p_c+1)(p_c+2)\kappa_{E,\Gamma}, \tag{24}$$

where $\kappa_{E,\Gamma} = \mathbf{n}_\Gamma \mathbf{D}_E^* \mathbf{n}_\Gamma$ represents the normal dispersion on Γ and $\sigma_0^t \geq 0$ is a user-dependent parameter. Despite the natural skew-symmetry of the advection-dispersion operator, we have included the additional symmetry term of the dispersive operator which is controlled here by the parameter ϵ_t. The resulting DG method is also called IIP, SIP, and NIP discretizations of the solute transport problem if ϵ_t is equal to 0, 1, and -1, respectively [18, 48, 68].

3.4. Time-discretization of coupled flow-transport problem

The IPDG approach for solving the coupled flow-transport process yields to a set of differential and algebraic equations. To this aim, let us consider the discrete variables $\varphi_h(\cdot,t) \in \mathcal{V}_h^{p_\varphi}$ and $c_h(\cdot,t) \in \mathcal{V}_h^{p_c}$ that we decompose as follows:

$$\varphi_h = \sum_{i=1}^{N_{\text{f}}} \varphi_i(t) v_i \quad \text{and} \quad c_h = \sum_{i=1}^{N_{\text{c}}} c_i(t) w_i \tag{25}$$

where $N_{\text{f}} = \dim(\mathcal{V}_h^{p_\varphi})$ and $N_{\text{c}} = \dim(\mathcal{V}_h^{p_c})$. Here, $(v_i)_{i=1,\dots,N_{\text{f}}}$ and $(w_i)_{i=1,\dots,N_{\text{c}}}$ denote the set of trial functions of approximation spaces $\mathcal{V}_h^{p_\varphi}$ and $\mathcal{V}_h^{p_c}$, respectively. The matrix form of the global discrete problem can be recast as follows:

$$\begin{bmatrix} \mathbb{S} & \mathbb{C} \\ 0 & \mathbb{T} \end{bmatrix} \begin{bmatrix} \dot{\boldsymbol{\varphi}}_h \\ \dot{\boldsymbol{c}}_h \end{bmatrix} + \begin{bmatrix} \mathbb{A}^{(\epsilon_f)} & 0 \\ 0 & \mathbb{B}^{(\epsilon_t)} \end{bmatrix} \begin{bmatrix} \boldsymbol{\varphi}_h \\ \boldsymbol{c}_h \end{bmatrix} = \begin{bmatrix} \boldsymbol{L}_{\text{f}} \\ \boldsymbol{L}_{\text{t}} \end{bmatrix} \tag{26}$$

where the *dot* symbol denotes the partial time-derivative operator, and $\boldsymbol{\varphi}_h^t = [\varphi_1, \ldots, \varphi_{N_\mathrm{f}}]$ and $\boldsymbol{c}_h^t = [c_1, \ldots, c_{N_\mathrm{c}}]$, the vector of degrees of freedom of the discrete variable φ_h and c_h, respectively. The block-matrices associated with (26) are given by,

$$\mathbb{S}_{|ij} = (s^*(c_h)v_j, v_i)_{\mathcal{E}_h}\,, \tag{27a}$$

$$\mathbb{C}_{|ik} = (\beta_0^*(c_h)w_k, v_i)_{\mathcal{E}_h}\,, \tag{27b}$$

$$\mathbb{T}_{|kl} = (\gamma(c_h)w_l, w_k)_{\mathcal{E}_h}\,, \tag{27c}$$

$$\mathbb{A}_{|ij}^{(\epsilon_f)} = a_h^{(\epsilon_f)}\,(v_j, v_i; c_h)\,, \tag{27d}$$

$$\mathbb{B}_{|kl}^{(\epsilon_t)} = b_h^{(\epsilon_t)}\,(w_l, w_k; \tilde{\mathbf{q}}_h^*)\,, \tag{27e}$$

$$\boldsymbol{L}_{\mathrm{f}|i} = l_f^{(\epsilon_f)}\,(v_i; c_h)\,, \tag{27f}$$

$$\boldsymbol{L}_{\mathrm{t}|k} = l_t^{(\epsilon_t)}\,(w_k; \tilde{\mathbf{q}}_h^*)\,. \tag{27g}$$

where indexes $i, j = 1, \ldots, N_\mathrm{f}$, $k, l = 1, \ldots, N_\mathrm{c}$, and block-matrices $\mathbb{A}, \mathbb{S} \in \mathbb{R}^{N_\mathrm{f}} \times \mathbb{R}^{N_\mathrm{f}}$, $\mathbb{B}, \mathbb{T} \in \mathbb{R}^{N_\mathrm{c}} \times \mathbb{R}^{N_\mathrm{c}}$, and $\mathbb{C} \in \mathbb{R}^{N_\mathrm{f}} \times \mathbb{R}^{N_\mathrm{c}}$. Due to the discontinuous nature of $\mathcal{V}_h^{p_\varphi}$ and $\mathcal{V}_h^{p_c}$, all computations (matrix assembly) can be done locally at the element level. We underline that the IPDG method leads to a very compact discretization stencil consist of a given mesh element and its direct neighbors. A popular way for solving the coupled differential-algebraic system (26) consists in splitting the numerical treatment of both physical sub-processes (flow and transport) and to treat them sequentially via an adapted flux reconstruction. Usually, for each time step, an iterative procedure is applied between the flow and transport operators until convergence. This approach could be more efficient in CPU time than the fully coupled approach that proceeds by solving both flow and transport operators simultaneously. However, the slow convergence of the iterative procedure between both operators affects significantly the performance of the solution. To avoid this problem, we use the non-iterative approach suggested by Younes and Ackerer [89]. In this paper, the time discretization is performed by a first-order Backward Differentiation Formula (BDF_1) and a direct solver using an unsymmetric-pattern multifrontal method and a direct sparse LU factorization (UMFPACK) is implemented for solving linear systems. Accuracy of the time discretization is insured using a proper time step management where the time step length is controlled by the temporal truncation error. Note that high order BDF can also be used and allow large time steps which may further improve the efficiency of the simulations [92]. The main steps of the non-iterative procedure used to solve the coupled flow and transport operators are described here. We denote by c_h^n and φ_h^n the discrete approximation of $c(\cdot, t_n)$ and $\varphi(\cdot, t_n)$ at the instant t_n with $0 \leq n \leq N$, respectively. Similarly, we denote by $\boldsymbol{\varphi}_h^n$ and $\boldsymbol{c}_h^n$ the corresponding vector of degrees of freedom. We describe below the staggered procedure for switching from t_n to t_{n+1} and calculating the $(n+1)$-th time step Δt^{n+1}.

- **Step 1.** Solve the transport problem: Given $\boldsymbol{c}_h^n$ and $\hat{\mathbf{q}}_h^{*\,n}$, seek $\boldsymbol{c}_h^{n+1}$ solving the equation,

$$\left[\frac{\mathbb{T}(\boldsymbol{c}_h^n)}{\Delta t^n} + \mathbb{B}^{(\epsilon_t)}(\hat{\mathbf{q}}_h^{*\,n})\right]\boldsymbol{c}_h^{n+1} = \boldsymbol{L}_\mathrm{t}(\boldsymbol{c}_h^n) + \frac{\mathbb{T}(\boldsymbol{c}_h^n)}{\Delta t^n}\boldsymbol{c}_h^n, \tag{28}$$

where $\Delta t^n = t_{n+1} - t_n$.

- **Step 2.** Solve the flow problem: Given initial values $\boldsymbol{c}_h^{n+1}$, seek $\boldsymbol{\varphi}_h^{n+1}$ solving the equation,

$$\left[\frac{\mathbb{S}(\boldsymbol{c}_h^{n+1})}{\Delta t^n} + \mathbb{A}^{(\epsilon_f)}(\boldsymbol{c}_h^{n+1})\right]\boldsymbol{\varphi}_h^{n+1} = \boldsymbol{L}_{\mathrm{f}}(\boldsymbol{c}_h^{n+1}) + \frac{\mathbb{S}(\boldsymbol{c}_h^{n+1})}{\Delta t^n}\boldsymbol{\varphi}_h^{n} - \frac{\mathbb{C}(\boldsymbol{c}_h^{n+1})}{\Delta t^n}(\boldsymbol{c}_h^{n+1} - \boldsymbol{c}_h^{n}). \tag{29}$$

- **Step 3.** Flux reconstruction: Given $\boldsymbol{c}_h^{n+1}$ and $\boldsymbol{\varphi}_h^{n+1}$, we reconstruct the global velocity field $\tilde{\mathbf{q}}_h^{*\,n+1} = [\mathbf{q}_h^{*\,n+1}, \hat{\mathbf{q}}_h^{*\,n+1}]$ on the whole domain as follows :

  - Mesh element: For all $A \in \mathcal{E}_h$, we compute interior approximations as follows,

$$\mathbf{q}_h^{*\,n+1} = -\mathbf{K}^*(c_h^{n+1})\left(\nabla\varphi_h^{n+1} + \beta_0 c_h^{n+1}\nabla z\right). \tag{30}$$

  - Mesh skeleton: For all $\Gamma \in \mathcal{F}_h^0$, we compute boundary approximations as follows,

$$\hat{\mathbf{q}}_h^{*\,n+1} = \begin{cases} \{\!\{\mathbf{q}_h^{*\,n+1}\}\!\} + \sigma_\Gamma^f \left[\!\left[\varphi_h^{n+1}\right]\!\right], & \text{if} \quad \Gamma \in \mathcal{F}_h^I, \\ \mathbf{q}_h^{*\,n+1} + \sigma_\Gamma^f\left(\varphi_h^{n+1} - \varphi_D^{n+1}\right)\mathbf{n}_\Gamma, & \text{if} \quad \Gamma \in \mathcal{F}_h^D. \end{cases} \tag{31}$$

- **Step 4.** Update the time step: The truncation error $\boldsymbol{e}^{n+1}$ measures the difference between first- and second-order temporal approximations of the concentration [89]:

$$\boldsymbol{e}^{n+1} := \frac{1}{2}\left[\boldsymbol{c}_h^{n+1} - \left(\boldsymbol{c}_h^{n} + \frac{\Delta t^n}{\Delta t^{n-1}}(\boldsymbol{c}_h^{n} - \boldsymbol{c}_h^{n-1})\right)\right]. \tag{32}$$

The uniform norm $\left\|\boldsymbol{e}^{n+1}\right\|_\infty$ is used to accept or reject the time step with respect to the user tolerance γ^{tol} (set at 10^{-3} in this work).

  - If $\left\|\boldsymbol{e}^{n+1}\right\|_\infty \leq \gamma^{\mathrm{tol}}$, the time step is accepted and the next one is estimated using,

$$\Delta t^{n+1} = \Delta t^n \min\left(\kappa\sqrt{\frac{\gamma^{\mathrm{tol}}}{\left\|\boldsymbol{e}^{n+1}\right\|_\infty}}, r_{\max}\right), \tag{33}$$

    where $\kappa(= 0.95)$ is a safety factor and $r_{\max}(= 2)$ is the maximum allowed time step.

  - Else, the time step is repeated with a smaller step size using the latest error estimate:

$$\Delta t_{j+1}^n = \Delta t_j^n \max\left(\kappa\sqrt{\frac{\gamma^{\mathrm{tol}}}{\left\|\boldsymbol{e}_j^{n+1}\right\|_\infty}}, r_{\min}\right), \tag{34}$$

    where j indexes the consecutive time step estimates and $r_{\min}(= 0.1)$ is the minimum allowed time step.

- **Step 5.** Update the initial guess: $n \leftarrow n+1$, $\boldsymbol{c}_h^n \leftarrow \boldsymbol{c}_h^{n+1}$, $\boldsymbol{\varphi}_h^n \leftarrow \boldsymbol{\varphi}_h^{n+1}$, $\Delta t^n \leftarrow \Delta t^{n+1}$ and back to **Step 1**.

3.5. Compatibility analysis & Frolkovič-Knabner procedure

Traditional algorithms employ operator-splitting to treat the coupled flow and transport processes sequentially and separately. However, when solving coupled processes, the discretization method employed to solve the flow is crucial since the approximate velocity field can strongly influence the positive features of the transport method. In 2003, Dawson et al. [16] analyzed compatible DG-algorithms for the coupled flow and transport problem. Specifically, they established some minimal requirements on the flow DG schemes to maintain optimal accuracy and conservation properties of the DG algorithms used for transport. Firstly, the authors proved that DG methods employed for the transport process must imperatively respect the *zero-order accuracy* requirement. This latter condition measures the ability of the DG method to reproduce a constant field by replacing the true velocity field $\mathbf{q}^*$ by its discrete approximation $\tilde{\mathbf{q}}_h^*$ in the transport process. Particularly, Sun and Wheeler [79] analyzed this criterion in the context of primal IPDG methods, and they established that all schemes namely, IIP-, NIP- and SIP-DG variants, verify it. However, it also imposes that the discrete velocity field verifies a *compatibility* requirement, implying that the DG method employed for the resolution of flow can not be chosen arbitrarily i.e.,

$$(\mathbf{q}_h^*, \nabla w_h)_{\mathcal{E}_h} + \langle \hat{\mathbf{q}}_h^*, [\![w_h]\!] \rangle_{\mathcal{F}_h} = \langle \mathbf{q}^* \cdot \mathbf{n}_\Gamma, w_h \rangle_{\mathcal{F}_h^{\text{in}}} \qquad \forall w_h \in \mathcal{V}_h^{p_c}. \tag{35}$$

Let us note that the *compatibility* condition (35) corresponds here to a stronger form of the local conservative principle since it holds for any polynomial functions in the space $\mathcal{V}_h^{p_c}$, and not only for piecewise constants. Thus, in virtue of (35), the IIP-DG scheme method for flow is the only one compatible with primal IPDG methods for transport in the sense defined in [16]. In compliance with Sun and Wheeler [79], the total number of permissible combinations to solve VDF equations is now reduced from nine to three compatible ones: IIP-IIP, IIP-SIP, and IIP-NIP. Any other combination of (non-compatible) methods can cause severe struggles such as a loss of accuracy or conservative properties, and may not even converge. For solving the VDF equations, we can choose related polynomial degrees of approximation for flow and transport i.e., $p_\varphi \sim p_c$, however, optimal or nearly optimal solution convergence can be attained when $p_\varphi = p_c$, in coupled flow and transport processes [79].

Besides, in buoyancy-driven problems, existence of additional gravity term in Darcy's velocity make a constraint on use of equal degrees of approximation for flow and transport due to the confliction between the head gradient and gravity terms of Darcy in parts of the domain where the velocity is zero or nearly zero [see e.g. 20, 32, 85]. To overcome this problem, a consistent velocity approximation based on Frolkovič-Knabner (FK) approximation [32] was developed for the IPDGs presented here for different polynomial degrees. The FK allows us to approximate flow and transport with the same degree of polynomials and also reduces the computational effort, considerably.

4. Results and discussion

A new numerical scheme is developed to solve the VDF equations with the DG method. This scheme is implemented in a numerical code. The first goal of this section is to validate the new developed scheme and to verify the correctness of the developed code. To do so, we use common benchmarks dealing with different configurations and applications of VDF and we compare the results of the new code against experimental results and semi-analytical solutions. The first benchmark is the Goswami-Clement laboratory experimental problem [35] that deals with saltwater intrusion in a rectangular experimental tank. This problem is used to test the new developed code in the case of specified-head boundary conditions (Dirichlet type). The comparison against experimental data would give an overall assessment of the robustness of the mathematical model in reproducing physical processes but cannot confirm the accuracy of the developed numerical solution and the correctness of the developed numerical code. The later can be well assessed by comparing numerical results against exact-analytical solutions. As there is no analytical solution for the VDF model, we compare the results of the new developed code against the semi-analytical solution of the Henry problem [39], which is a common benchmark for seawater intrusion. Several semi-analytical solutions of the Henry problem have been suggested in the literature [39, 71, 75, 90, 95], here we use the recent solution developed by Fahs et al. [28] as, in contrast to the previous solutions, it involves velocity-dependent dispersion. The Henry problem allows not only comparison against semi-analytical solution but also checking the model in a case dealing with specified-flux boundary conditions (Neumann type). Both Goswami-Clement and Henry problems deal with mixed convection as the flow is generated by a head gradient or forced conditions. In order to investigate the new developed code in a case involving purely natural convection, we consider the problem of natural convection in porous square cavity with vertically heated walls. In this case, VDF is thermally driven. The flow is generated by the temperature gradient. This problem is commonly used to represent natural convection in porous media in either cases of vertical (horizontally heated walls) or horizontal temperature gradient (vertically heated walls). We do not consider horizontally heated wall as the problem could be unstable. Unstable problems are not suitable for benchmarking as they could have multiple solutions [65]. Our new developed code is compared against the stable semi-analytical solution developed by [29]. For validation, we consider cases dealing with relatively small Rayleigh number. Beside verification, the problem of porous square cavity would also highlight the flexibility of the new developed model in treating either solute or thermal problems and even coupled thermohaline problems.

The Results section aims also at highlighting the performance and accuracy of the developed DG scheme in solving VDF equations. To do so, we consider a case of the porous cavity problem with high Rayleigh number and we compare the new developed model against a commercial model based on standard finite element method (COMSOL Multiphysics). Fahs et al. [29] have shown that such a case is computationally challenging as accurate solution of this case is beyond the capacity of current models. Standard numerical techniques used in current models could lead to spurious oscillations or numerical diffusion.

4.1. Validation: The Goswami-Clement experimental problem

Herein, to validate our model we simulate the laboratory experiments originally performed by Goswami and Clement [35]. These experiments have been developed with the purpose of evaluating the density-dependent models. The experimental setup composed of a rectangular flow tank comprising three distinct chambers. The central chamber contains an unconfined, homogeneous, porous medium and two constant-head chambers on the left and right sides containing saltwater and freshwater, respectively. Goswami and Clement [35] completed their experiments by recording the data in both transient and steady state conditions. As a result, in addition to the steady state validation, the transient test of numerical models is also possible. The saltwater intrusion experiments were conducted under three transient phases ended with steady state conditions. The first phase was established by setting the right freshwater head equal to 26.7 cm and fixing the left equivalent freshwater head proportional to the saltwater head of 25.5 cm. Under these conditions, the first steady state condition (SS_1) was obtained for the salt wedge (initial phase). Then the freshwater head was instantaneously reduced to 26.2 cm and maintained until the second steady state condition (SS_2) is reached (advancing phase). Finally, the freshwater head was increased to 26.55 cm which forces the salt wedge to recede and the conditions was kept until the third steady state condition (SS_3) was established (receding phase).

In the present study, we tested our DG model by comparing the simulation results against experiments data in both transient and steady state conditions. For numerical simulations, the unconfined porous medium was assumed to be confined with the boundary conditions depicted in Fig. 2, [35]. The domain was discretized using $44K$ structured right-angled triangles with equal grid spacing and linear polynomial approximations were used for both variables i.e., head and mass fraction. The initial mass fraction and freshwater head were set to zero and 26.7 cm, respectively. Table 1 illustrates the physical parameters used for simulation of the experiments.

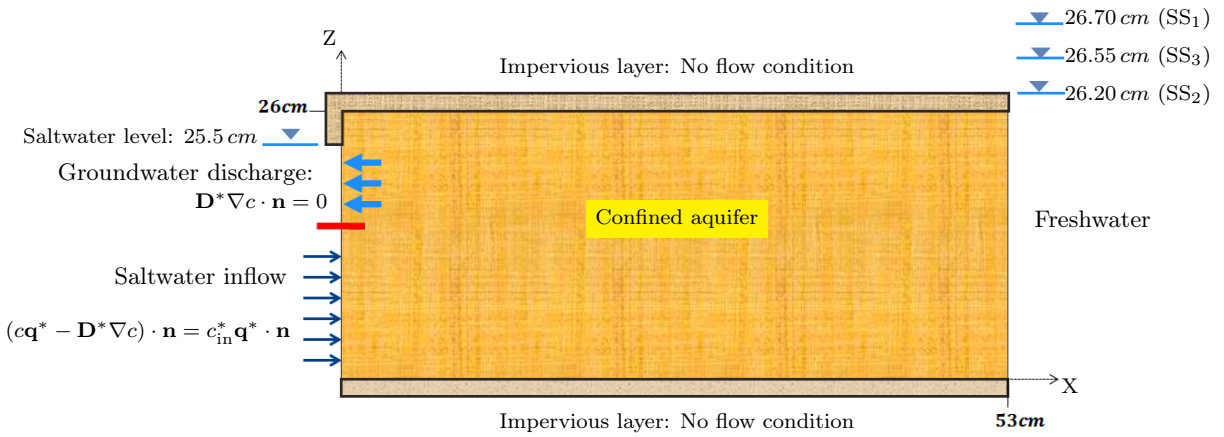

Fig. 2. Geometry and boundary conditions for the Goswami-Clement experimental setup

Fig. 3 illustrates the 10, 50 and 90 % isochlors predicted in steady state condition for three phases, SS_1

Table 1. Physical parameters for the Goswami-Clement experimental problem

Parameter	Value	Unit
K	0.0122	ms^{-1}
D_m	1.0×10^{-9}	$m^2 s^{-1}$
α_L	0.001	m
α_T	0.0001	m
s	1.0×10^{-5}	m^{-1}
ϕ	0.385	–
ρ_0	1000	$kg\ m^{-3}$
ρ_s	1026	$kg\ m^{-3}$
μ_0	0.001	$kg\ m^{-1}\ s^{-1}$
β_μ	0	–
β_0	0.026	–

to SS_3. In addition to the experimental data from measurements of salt wedge location, the numerical results of SEAWAT [35] were superimposed for comparison. As can be seen, our results are in excellent agreement with the experimental data. The maximum difference between the results and experimental data respects to SS_2. This is while for the SEAWAT model, the difference exists for all the three steady state conditions. In general, our model can provide a closer prediction of salt wedge, particularly in the toe, for SS_1 to SS_3. Note that the results from IIP-IIP, IIP-SIP and IIP-NIP were closely similar [67].

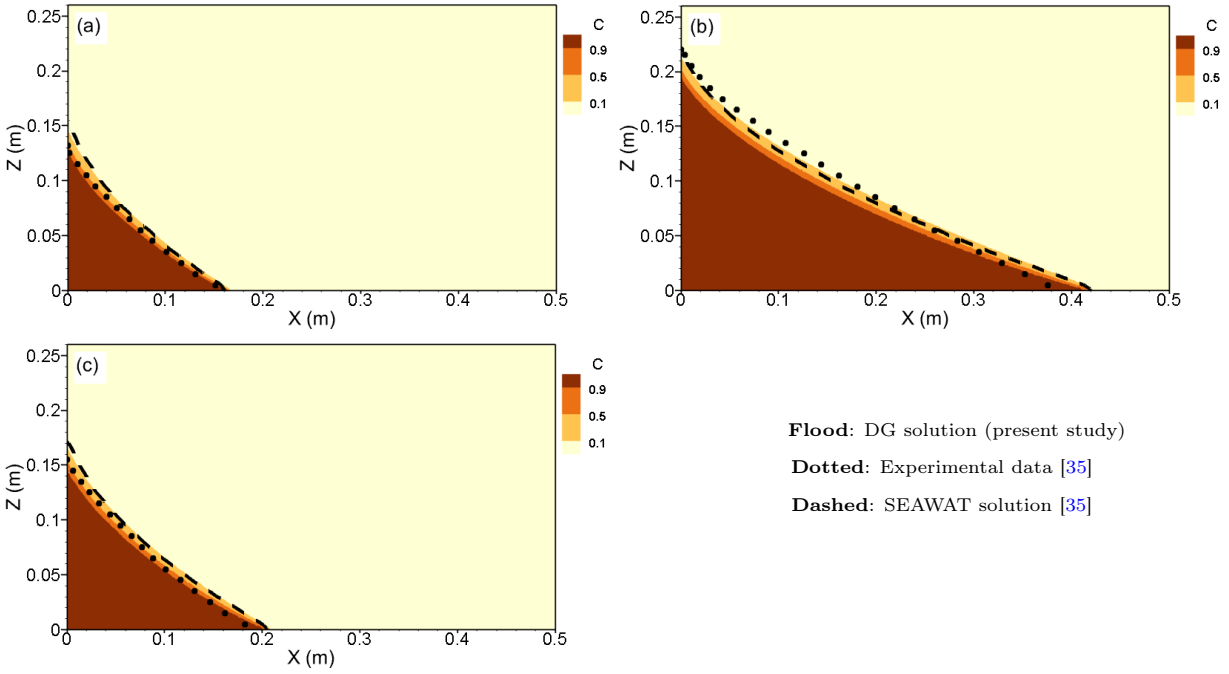

Fig. 3. 10%, 50% and 90% isochlors of DG solution in comparison with Goswami experimental data [35] and 50% SEAWAT isochlor [35] in the (a) first steady state (SS_1), (b) second steady state (SS_2), and (c) third steady state (SS_3) conditions

Here, for the first transient test, the advancing phase of salt wedge was also considered. Fig. 4 compares the results of numerical simulations with experimental measurements at times 5, 15, 55 *min* after starting the second phase. Similar to the steady state test, the results match well with the experimental data at the

different times. The results show that the more salt wedge advances over time, the less agreement appears due to approaching to SS_2 position. The results of SEAWAT model were also presented in the figure for comparison. Similarly, for SEAWAT, the differences was increased in the later times. As a second part of transient test, we performed a comparison of numerical results with experimental data in receding phase. Again, the most difference is observed when the salt wedge is closer to SS_2 position (Fig. 5). This condition is also true for SEAWAT [67].

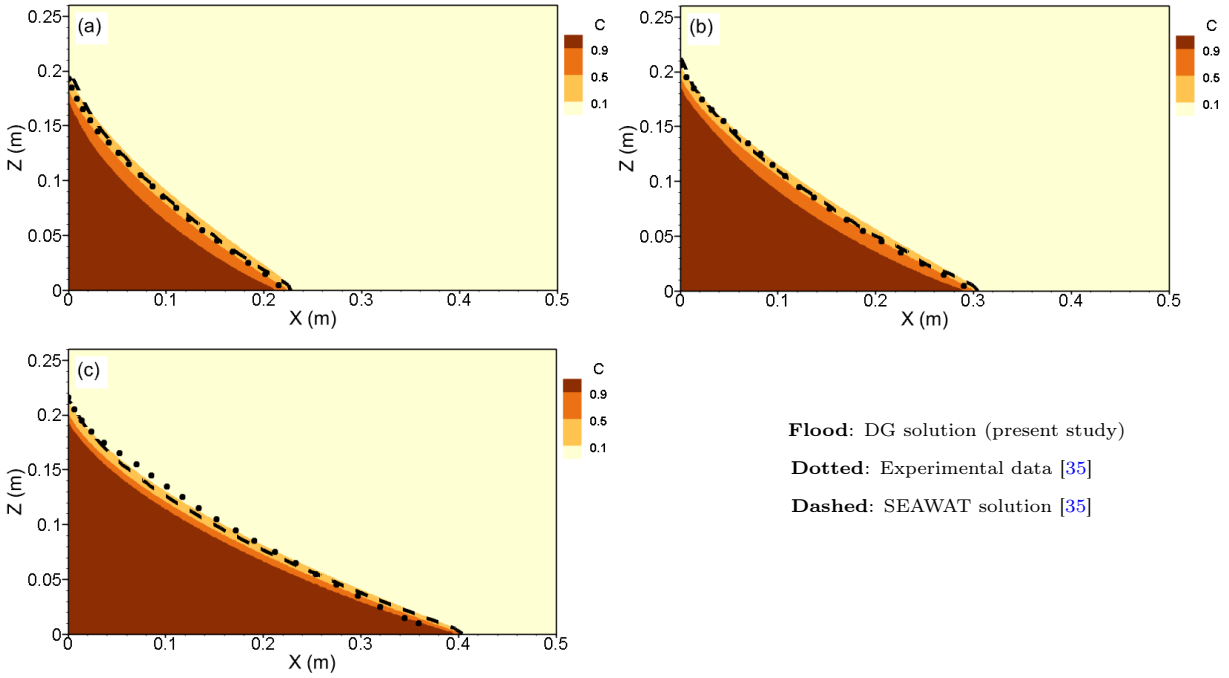

Fig. 4. 10%, 50% and 90% isochlors of DG solution in comparison with Goswami experimental data [35] and 50% SEAWAT isochlor [35] at (a) 5 min, (b)15 min, and (c) 55 min of advancing phase (moving from SS_1 toward SS_2)

Finally, a flux test was also presented to compare the freshwater fluxes predicted by the model against the steady state flux measurements. Table 2 reports the measured fluxes and the results from our DG code and SEAWAT. For the DG, the most difference is happened in SS_3, though, this is not significant and is less than 2 percent. Generally, the fluxes estimated by our model compared to SEAWAT have closer agreement with the experimental measurements.

Table 2. Numerical fluxes ($cm^3 \cdot s^{-1}$) in comparison with the experimental data and SEAWAT for the three steady state conditions of Goswami-Clement problem

	SS_1	SS_2	SS_3
Experimental measurement [35]	1.42	0.59	1.19
DG (present study)	1.41	0.6	1.17
SEAWAT [35]	1.46	0.59	1.13

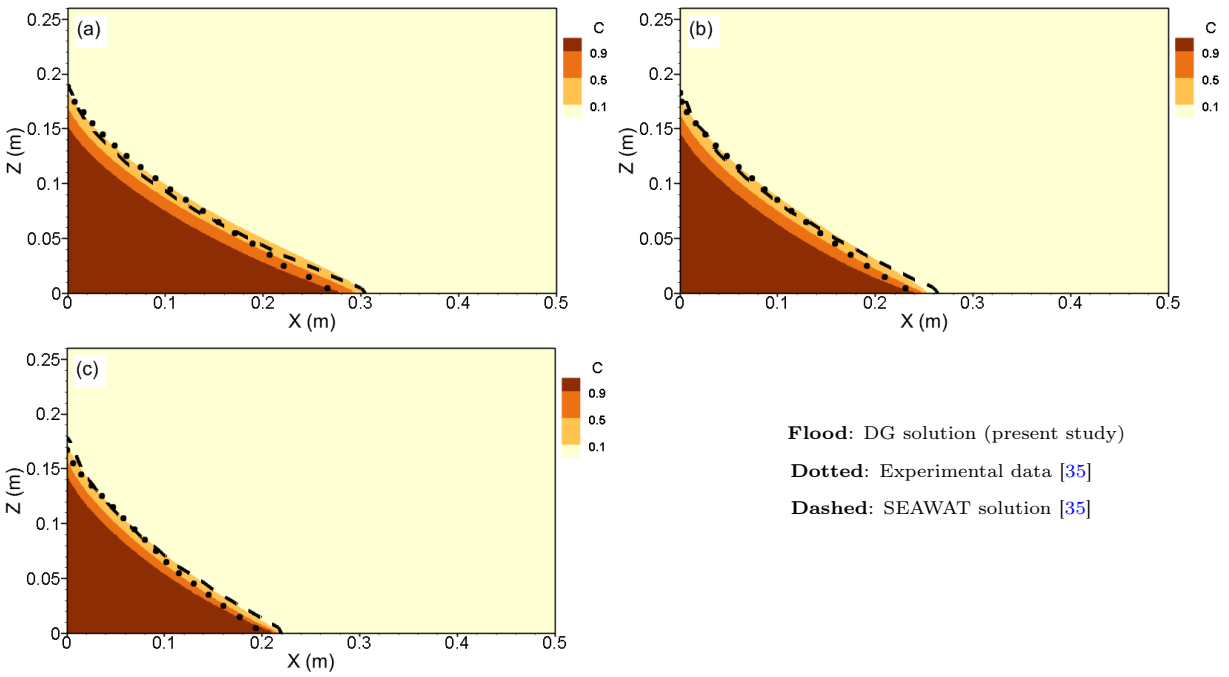

Fig. 5. 10%, 50% and 90% isochlors of DG solution in comparison with Goswami experimental data [35] and 50% SEAWAT isochlor [35] at (a) 10 min, (b)15 min, and (c) 25 min of advancing phase (moving from SS_2 toward SS_3)

4.2. Verification against semi-analytical solution: The Henry problem

Henry [39] was the first to model seawater intrusion phenomenon in a variable density system. His simplified rectangular model is constructed based on a confined, homogeneous, isotropic 2D aquifer in a vertical section (Fig. 6). As shown, the left landward boundary is recharged by a constant rate of freshwater (Q) and the right boundary is ended to the sea such that the top aquifer boundary is just leveled at the sea surface. Saltwater intrudes from the seaside until an equilibrium is established with the landward inflowing freshwater. Henry developed a semi-analytical solution based on the double Fourier series for the problem under the steady state condition. Due to the availability of the analytical solution, for many years, various attempts have been made [see the review in 76, 95] aimed at utilizing the Henry problem as benchmark for variable density flow models. The first semi-analytical solution, developed by Henry [39], has been limited to high diffusion for which the buoyancy processes are dominated by diffusion. Voss et al. [84] showed that this solution is a necessary but not a sufficient test for a simulator to present variable-density physics. Several further studies suggested new semi-analytical solutions that are more sensitive to the variable-density flow physics by reducing the imposed inland flow or the diffusion coefficient [76, 91, 95].

Here we use the semi-analytical solution developed by Fahs et al. [28] that includes velocity-depended dispersion. This solution is more realistic than previous solutions in representing seawater intrusion processes. It is more suitable for code verification as it includes velocity dependent dispersion. Here for verification purposes, we consider the three cases presented in Fahs et al. [28]. The first one is similar to the standard solution suggested by Henry [39]. It deals with pure molecular diffusion. The second one in-

cludes velocity-dependent dispersion, but with exaggerated dispersion coefficients leading to a wide mixing zone. These two cases are relatively simple from computational point of view as they do not involve sharp solutions. They are useful in verifying the correctness of the developed code. The third case deals with small dispersion coefficients, leading to a very narrow mixing zone. As shown in Fahs et al. [28], this case is computationally challenging because of its high sensitivity to the numerical scheme. Fahs et al. [28] showed that, for this case, standard finite element method leads to inaccurate results due to numerical diffusion. The physical parameters used in the three test cases are given in Table 3. Note that the three cases can be derived from the standard Henry problem by changing one or more of the following parameters: domain length (l), molecular diffusion (D_m) and dispersion coefficients (α_L , α_T).

For the purpose of numerical solution, following Fahs et al. [28], the domain was discretized using structured meshes comprising 7500, 12288 and 76800 triangles for test cases 1 to 3, respectively. For all the test cases except the third one which utilizes quadratic polynomial for head, the linear polynomial approximations were applied for both variables. The imposed boundary conditions are depicted in Fig. 6. All combinations of DG schemes are used for the simulation of Henry problem, however, we observed no significant difference between the results. Main isochlors (10%, 50% and 90%) as well as the velocity field for the three test cases are represented on Fig. 7. It can be observed that there is an excellent agreement between generated DG isochlors and those of semi-analytical solution throughout the total aquifer thickness. The third case highlights the capacity of the developed DG solution in reproducing a narrow mixing zone that could be very sensitive to numerical dispersion [28]. A more quantitative comparison is performed using scalar indicators representing the seawater intrusion metrics. The results are summarized in Table 4. For test case 1, the difference between the DG and semi-analytical solutions is less than 1.5%. The highest difference is observed for the width of the mixing zone. The post treatment procedure used for the evaluation of this zone depends on the computational mesh. For the second and third test cases, the discrepancy between the solutions is less than 6%, except for the mixing zone and the total flux. The small discrepancies between the solutions regarding L_s and L_{toe} confirms that DG avoids the problem of numerical dispersion. In fact, numerical dispersion could overestimate the diffusion processes and leads to an overestimation of L_{toe} and L_s.

4.3. Verification against semi-analytical solution: The problem of natural convection in a porous enclosure

An important application of the VDF is in natural convection in porous enclosure. In this case, the density variation is related to a thermal gradient. This problem can be modeled by a system of equations equivalent to the solute VDF problems. For thermal problems, the porosity is analogue to the equivalent specific heat of the porous domain and the molecular diffusion is analogue to the equivalent thermal diffusivity of the porous domain. In thermal application, the expansion coefficient in (7), should be negative as the density decreases with the increase of temperature. Thus the developed DG scheme can be applied to solve thermal density-driven problems. The previous test cases deal with mixed convection as the flow

Table 3. Physical parameters used for the simulations of the three test cases of the Henry problem

Parameter	Value			Unit
	Case 1	Case 2	Case 3	
$\mathbf{K}$	$0.01 \times \mathbf{I}$	$0.01 \times \mathbf{I}$	$0.01 \times \mathbf{I}$	ms^{-1}
D_m	18.86×10^{-6}	9.43×10^{-8}	9.43×10^{-8}	$m^2 s^{-1}$
α_L	0.0	0.1	0.001	m
α_T	0.0	0.01	0.0001	m
s	0	0	0	m^{-1}
ϕ	0.35	0.35	0.35	–
ρ_0	1000	1000	1000	$kg\ m^{-3}$
ρ_s	1025	1025	1025	$kg\ m^{-3}$
Q	6.6×10^{-5}	6.6×10^{-5}	6.6×10^{-5}	ms^{-1}
μ	0.001	0.001	0.001	$kg\ m^{-1}\ s^{-1}$
β_0	0.025	0.025	0.025	–

Table 4. Computed seawater intrusion metrics for Henry test cases [28]

Metrics*	Test case 1		Test case 2		Test case 3	
	DG	Semi-analytical	DG	Semi-analytical	DG	Semi-analytical
L_{Toe}	0.624	0.624	1.246	1.256	1.604	1.594
L_s	0.752	0.751	0.393	0.368	0.087	0.088
W_{mz}	0.756	0.757	0.323	0.295	0.088	0.09
Z_1	0.425	0.419	0.51	0.527	0.691	0.684
Q_s	1.066	1.068	1.069	1.061	0.35	0.3

* Adapted from [28]:
L_{toe} is the dimensionless distance to the seaside boundary that seawater intrudes along the aquifer bottom (measured based on 50% isochlor),
L_s is the dimensionless distance between 10 and 90% isochlors along the aquifer bottom,
W_{mz} is the vertically dimensionless average width of the mixing zone,
Z_I is the dimensionless vertical coordinate of the point at which flow direction at seaside boundary alters adversely,
Q_s is the saltwater inflow flux from seaside boundary divided by freshwater recharge (Q) .

is either imposed or generated by an imposed pressure gradient. The main goal of this section is to test the new developed scheme in cases involving natural convection, where flow is induced by density gradient. Thus, we consider the well-known benchmark of natural convection in a porous cavity (Fig. 8). The domain of the problem is a unit square filled with homogeneous porous medium. All sides are impervious respective to fluid. Right and left sides of the domain have different temperatures with 1 and 0 dimensionless temperatures, respectively. Other boundary conditions and data are depicted in Fig. 8. The main factor of fluid density changes is the temperature differences due to heating the fluid from the boundaries. The convective flow and heat transfer processes are governed by the dimensionless Rayleigh number ($Ra = \mathbf{K}l\beta_0\Delta c/\phi D_m$, where l is the domain length) expressing the ratio of the buoyancy forces to the viscous-diffusion effects.

Fahs et al. [29] developed a semi analytical solution for this problem which is used here to verify the proposed DG scheme. We consider cases dealing with low and average Rayleigh numbers ($Ra = 100$ and $Ra = 1000$). The physical parameters used in the simulations are given in Table 5.

In the previous test for Henry problem, DG was evaluated for linear approximation. Here, higher order

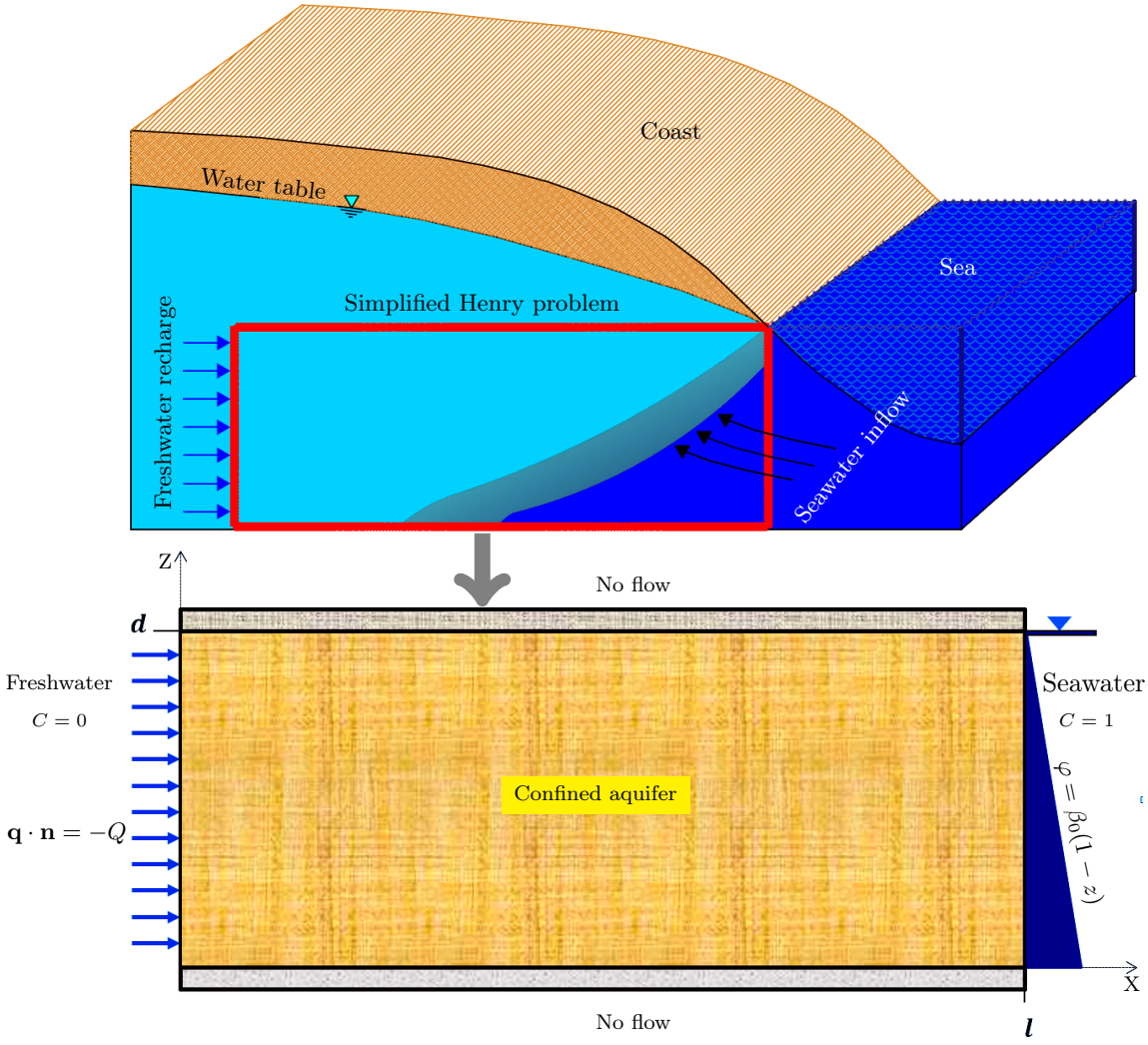

Fig. 6. Simplification of seawater intrusion by Henry [39] and the implemented boundary conditions

approximations of DG are examined. Accordingly, the domain is discretized by 2500 and 6400 uniform triangular elements for $Ra = 100$ and $Ra = 1000$, respectively, and the developed DG code is used for a wide range of polynomial degrees (from 1 to 4). The isotherms 0.2, 0.4, 0.6, 0.8 and the velocity field are depicted in Fig. 9 in comparison with those of semi-analytical solution of Fahs et al. [29]. This figure shows the occurrence of convective cells. The temperature gradient generates a clockwise rotating flow. The increase of the Rayleigh number accelerates the rotating flow. Convection dominates the heat transfer processes and the isotherms become more dependent on the flow structure. As can be seen, DG solution perfectly match the semi-analytical solutions.

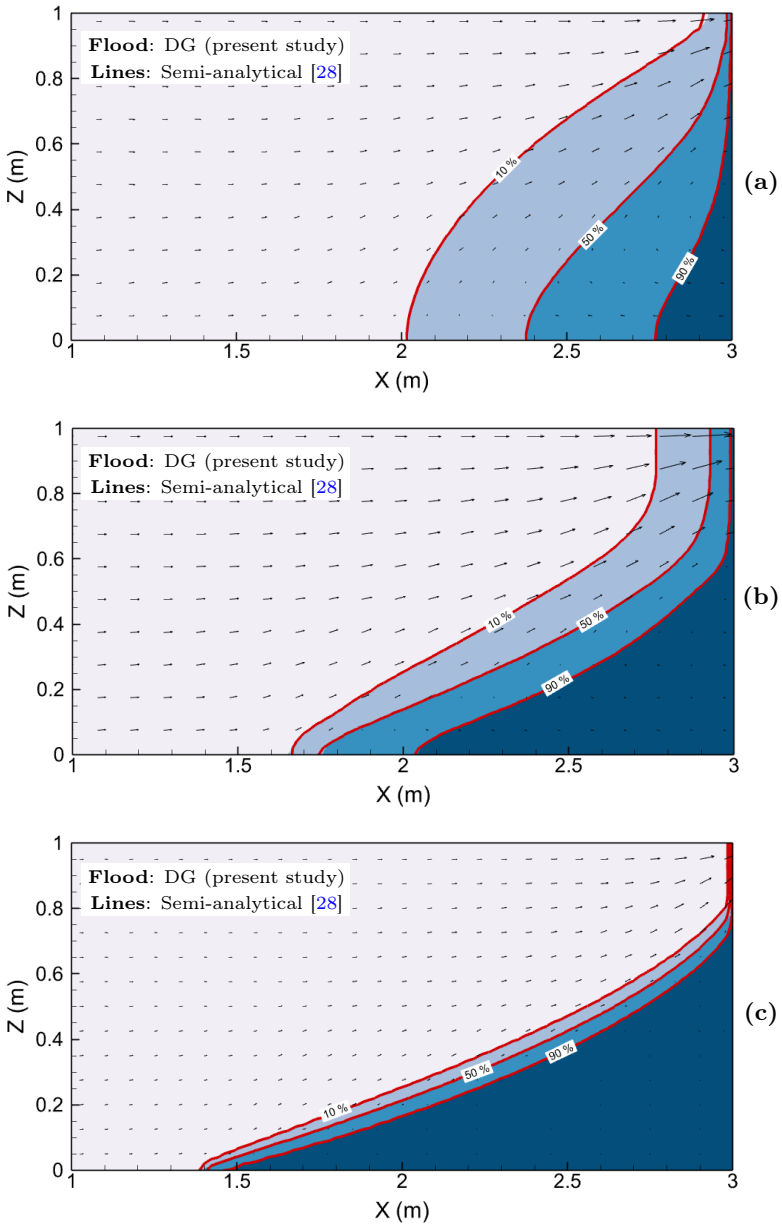

Fig. 7. Main iscohlors and velocity field for the test case 1 (a), test case 2 (b), and test case 3 (c) of the Henry problem: comparison between the DG and semi-analytical solutions

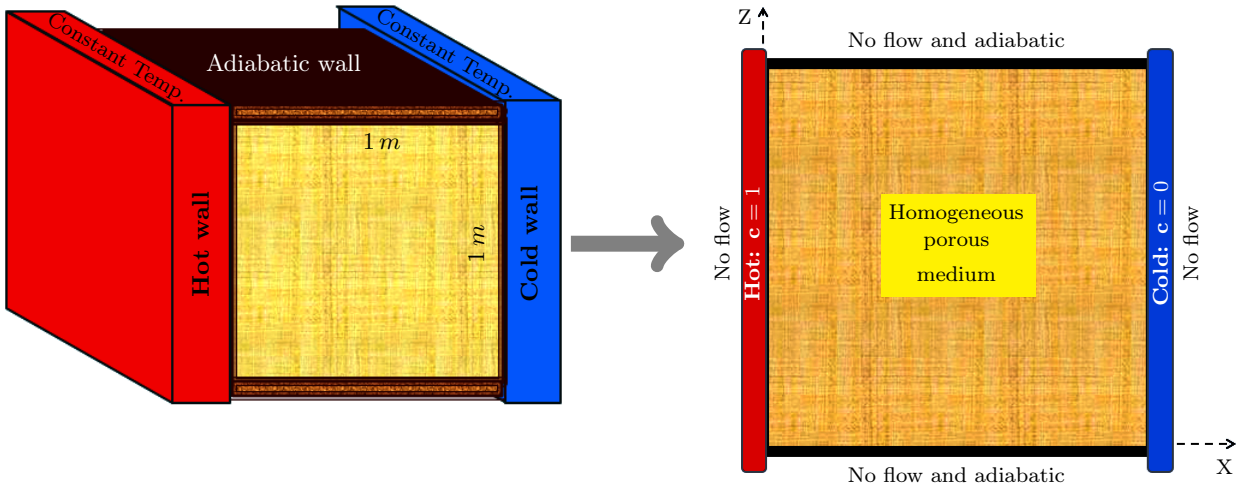

Fig. 8. Geometry and boundary conditions of the problem of natural convection in porous cavity

Table 5. Physical parameters for simulation of the problem of natural convection in porous cavity

Parameter	Value	Unit
$\mathbf{K}$	$0.01 \times \mathbf{I}$	ms^{-1}
D_m	1×10^{-6} ($Ra = 100$), 1×10^{-7} ($Ra = 1000$), 1×10^{-8} ($Ra = 10000$)	$m^2 s^{-1}$
α_L	0	m
α_T	0	m
s	0	m^{-1}
ρ_0	1000	$kg\ m^{-3}$
μ	0.001	$kg\ m^{-1}\ s^{-1}$
β_0	-0.01	$-$

4.4. Performance and accuracy of the developed DG solution: Natural convection with a high Rayleigh number

This section aims at examining the performance of the new developed DG scheme against conventional methods. Thus, we consider a computationally challenging case and we simulate this case with the DG scheme and with a standard finite element solution obtained using COMSOL. We simulate the case on natural convection in porous enclosure under high Rayleigh regime ($Ra = 10000$). Fahs et al. [29] showed that in this case, conventional numerical methods suffer from numerical dispersion and/or nonphysical oscillations. They showed that accurate simulation of this test case is beyond the capacity of conventional models. In their work, the author proposed a reference solution based on the Fourier series method. We simulate this case using the DG scheme and COMSOL. For the DG scheme we use a computational mesh of 10K elements and we test different polynomial orders from 1 to 4. In COMOS, we use two levels of mesh refinement consisting of about 100K and 600K elements. COMSOL simulations are performed with first polynomial order. We use the average Nusselt number to evaluate the performance of both models. The average Nusselt number represents the dimensionless heat flux to the domain. It is calculated by: $\overline{Nu} = \int_{\partial\Omega} Nu|_{x=0} = \int_{\partial\Omega} \nabla c|_{x=0} \cdot \mathbf{n}$ [29].

Table 6 summarizes the Nusselt number for the DG scheme in comparison with those of semi-analytical

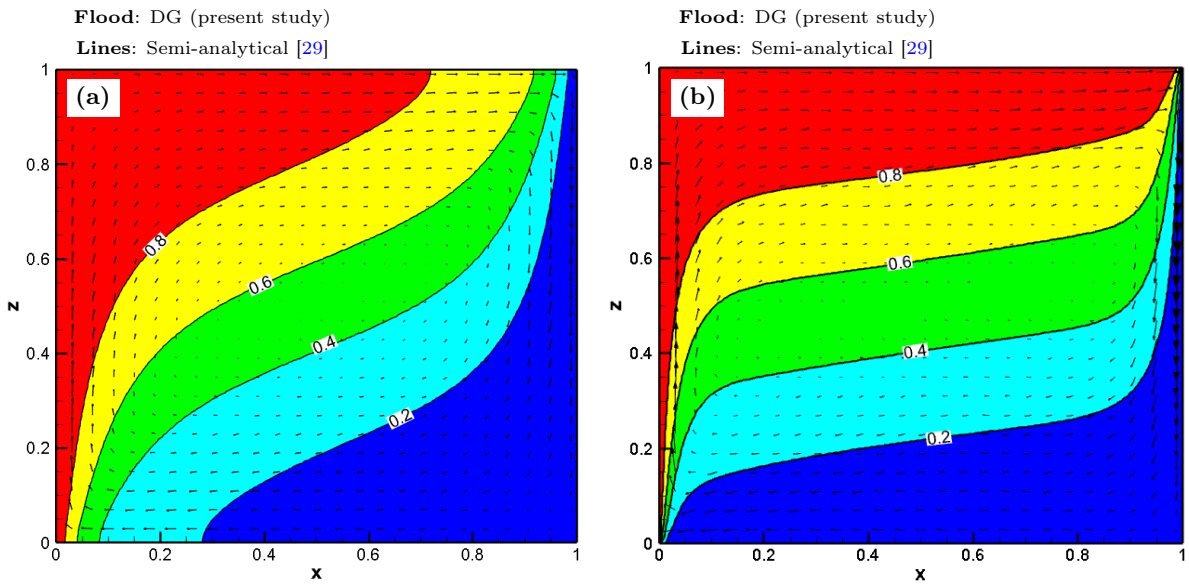

Fig. 9. Comparison of DG solution with that of semi-analytical for (a) $Ra = 100$ and $Ra = 1000$

Table 6. Nusselt number achieved for different number of DOFs per each variable

	DG				COMSOL-Multiphysics		Semi-analytical
	Order 1	Order 2	Order 3	Order 4	Order 1	Order 1	
Number of elements	10,000	10,000	10,000	10,000	100,110	655,752	–
Number of DOFs	60,000	120,000	200,000	300,000	201,022	1,313,506	–
$\overline{Nu}$	33.14	50.45	45.24	46.15	38.07	44.9	46.14

solution and COMSOL-Multiphysics. We should mention that, by default in COMSOL, second polynomial order is used for flow and first order is used for transport. As shown, the $\overline{Nu}$ achieved for DG approaches to that of analytical as the order of polynomial approximation (the number of DOFs) is increased until at order 4 including totally 300,000 DOFs, $\overline{Nu}$ is extremely close to analytical value. Fig. 10 pinpoints how the relative error on Nusselt number decreases as the number of DOFs is increased. COMSOL-Multiphysics is a standard finite element software and its results were also included to demonstrate how DG is superior to standard finite element method. We observe for high order DG solution, $\overline{Nu}$ is more close to the analytical value, though, less than a quarter of the number of COMSOL-Multiphysics' DOFs was used. The DG scheme intrinsically has less numerical dispersion and this is why a more accurate solution is achieved for, even with a much less number of DOFs. Fig. 11 depicts the isotherms for both models against the semi-analytical solution. As illustrated, DG isotherms (for order 4) have closer agreement with the semi-analytical solution than COMSOL.

The results of this test case show clearly a significant improvement in the accuracy of the solution due to the DG method. This is in agreement with several previous studies on flow and transport in porous media, confirming the high accuracy of the DG methods. However, in general the DG method is seen to be

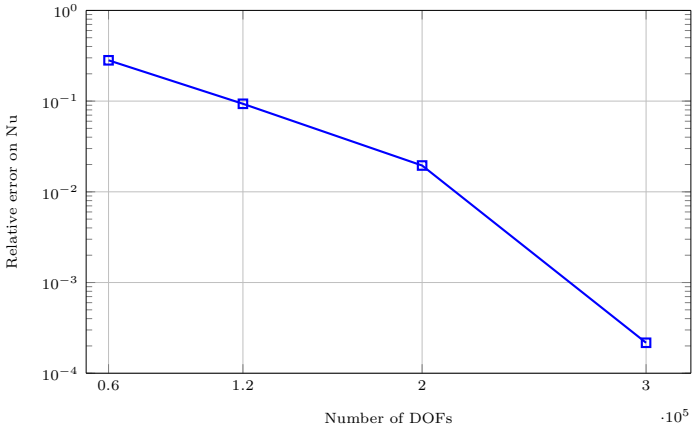

Fig. 10. Relative error on $\overline{Nu}$ versus number of DOFs

more consuming in CPU time and memory than standard methods, due to the high number of DOFs per element of the computational mesh. The results here show that for VDF problems, this is not totally true. In fact, a reliable comparison should respect the balance between computational efficiency and solutions accuracy. In this logic, Table 6 confirms the superiority of the DG methods for the simulation of VDF problems.

5. Conclusion

Several recent studies have highlighted the advantages of the DG methods in solving partial differential equations governing flow or transport processes in porous media. This method has been never used to solve the full system of VDF equations. Yet, simulations of VDF requires high accurate numerical methods as the accuracy of the numerical solutions is highly sensitive to the numerical scheme. The first objective of this work is to show how the equations of VDF can be solved with the DG method. This requires extension of the DG method to solve nonlinear equations coupling flow and convective/dispersive transport equations under variable density. We develop, in a unified format, the general class of Interior Penalty DG (IPDG) methods to solve VDF equations. We test symmetric, non-symmetric and incomplete IPDG methods to discretize both head and concentration variables. Numerical experiments are performed to validate the developed DG scheme and to examine its performance in solving VDF problems.

The developed numerical scheme is implemented in a numerical code which is used to simulate common benchmarks dealing with VDF. The simulations are performed to validate and verify the developed DG scheme. The benchmarks are selected to cover different types of boundary conditions and convective flow processes (either, mixed, natural, solute or thermal). Validation is performed by comparing the results of the developed DG scheme with experimental data, based on the Goswami-Clement experimental problem. Good agreement has been found. The new developed DG scheme reproduces the experimental data better than the finite element SEAWAT code. Verifications are performed by comparing the code against the semi-

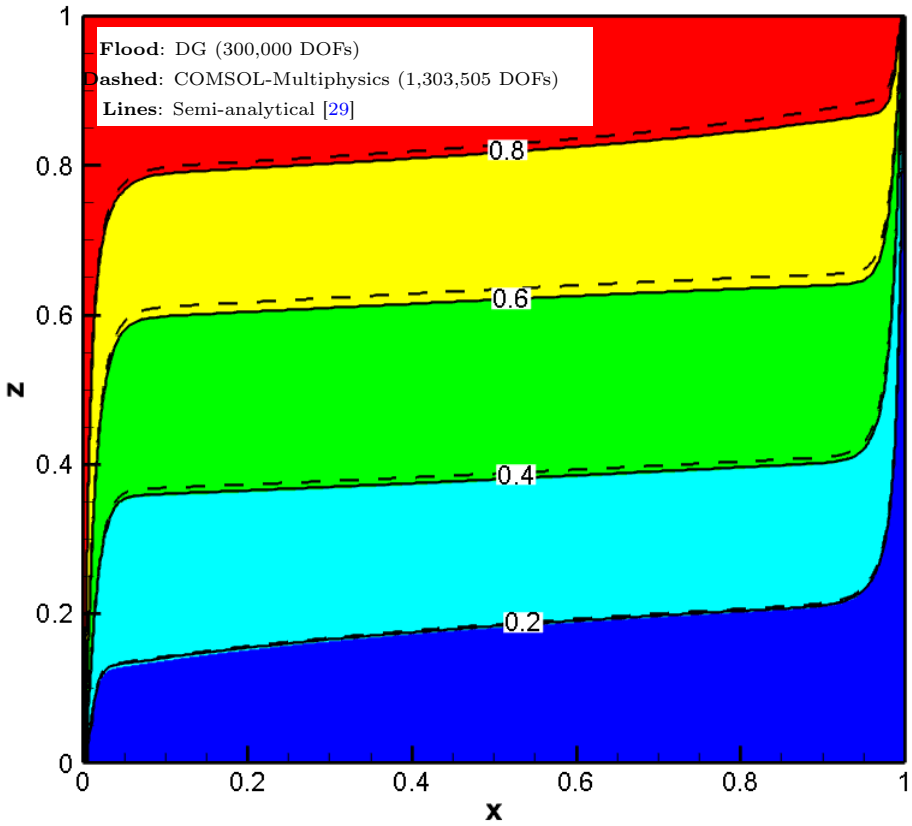

Fig. 11. Isotherms concluded from DG compared to that of analytical and COMSOL-Multiphysics

analytical solutions of the dispersive Henry problem dealing with seawater intrusion in coastal aquifers and the problem of thermal natural convection in a porous enclosure. Excellent agreement has been obtained with semi-analytical solutions for cases involving wide mixing zone or small Rayleigh numbers. This confirms the correctness of the developed code and DG scheme. Furthermore, close agreement has been obtained for Henry problem in the case of narrow mixing, which illustrates the promising results of the DG method in solving VDF with sharp fronts. These numerical experiments show that, whole algorithm combinations, i.e. IIP-IIP, IIP-SIP, and IIP-NIP have no significant differences in the solutions.

To highlight the performance of the DG method in solving the equations of VDF, we simulate the problem of natural convection at a high Rayleigh number (10,000). Accurate solution of this problem is out of the capacity of current models based on conventional methods. We compared the DG results to a semi-analytical solution and to a finite element solution obtained using COMOSL multi-physics. The results prove the promising performance of the DG method at high polynomial order as it provides higher accuracy than standard finite element method with reduced number of degree of freedom. The DG method outperforms the conventional method that we tested.

This study is the first step towards application of DG methods in the area of VDFs. Future work should target applying other nice properties of DG such as adaptivity in mesh and polynomial approximation

(hp-version) to even more reduce the computational cost. The proposed method is generic and can be extended to 3D, which is an ongoing research project of this work.

6. Acknowledgement

The authors would like to appreciate the use of the computational clusters of the High Performance Computing Center (ShahreKord University, Iran), to complete this work. The data used in this work are available on the GitHub repository: https://github.com/fahs-LHYGES

References

[1] Abbà, A., Bonaventura, L., Nini, M., Restelli, M., 2015. Dynamic models for Large Eddy Simulation of compressible flows with a high order DG method. Computers and Fluids 122, 209–222. doi:10.1016/j.compfluid.2015.08.021.

[2] Ackerer, P., 2004. A new coupling algorithm for density-driven flow in porous media. Geophysical Research Letters 31, L12506. URL: http://doi.wiley.com/10.1029/2004GL019496, doi:10.1029/2004GL019496.

[3] Ackerer, P., Younes, A., 2008. Efficient approximations for the simulation of density driven flow in porous media. Advances in Water Resources 31, 15–27. URL: http://www.sciencedirect.com/science/article/pii/S0309170807001054, doi:10.1016/j.advwatres.2007.06.001.

[4] Ackerer, P., Younes, A., Mose, R., 1999. Modeling variable density flow and solute transport in porous medium: 1. Numerical model and verification. Transport in Porous Media 35, 345–373. URL: https://link.springer.com/article/10.1023%2FA%3A1006564309167, doi:10.1023/A:1006564309167.

[5] Albets-Chico, X., Kassinos, S., 2013. A consistent velocity approximation for variable-density flow and transport in porous media. Journal of Hydrology 507, 33–51. URL: http://www.sciencedirect.com/science/article/pii/S0022169413007270, doi:10.1016/j.jhydrol.2013.10.009.

[6] Arbogast, T., Juntunen, M., Pool, J., Wheeler, M.F., 2013. A discontinuous Galerkin method for two-phase flow in a porous medium enforcing H(div) velocityand continuous capillary pressure. Computational Geosciences 17, 1055–1078. URL: https://link.springer.com/article/10.1007/s10596-013-9374-y, doi:10.1007/s10596-013-9374-y.

[7] Arnold, D.N., 1982. An interior penalty finite element method with discontinuous elements. SIAM Journal on Numerical Analysis 19, 742–760. URL: http://epubs.siam.org/doi/abs/10.1137/0719052, doi:10.1137/0719052.

[8] Arnold, D.N., Brezzi, F., Cockburn, B., Donatella Marini, L., 2001. Unified analysis of discontinuous Galerkin methods for elliptic problems. SIAM Journal on Numerical Analysis 39, 1749–1779. URL: http://epubs.siam.org/doi/abs/10.1137/S0036142901384162, doi:10.1137/S0036142901384162.

[9] Arnold, D.N., Brezzi, F., Cockburn, B., Marini, D., 2000. Discontinuous Galerkin Methods for Elliptic Problems, in: Discontinuous Galerkin Methods. Springer. volume 11, pp. 89–101. URL: http://link.springer.com/10.1007/978-3-642-59721-3_5, doi:10.1007/978-3-642-59721-3_5.

[10] Bastian, P., 2014. A fully-coupled discontinuous Galerkin method for two-phase flow in porous media with discontinuous capillary pressure. Computational Geosciences 18, 779–796. URL: http://link.springer.com/10.1007/s10596-014-9426-y, doi:10.1007/s10596-014-9426-y, arXiv:1309.7555.

[11] Baumann, C.E., Oden, J.T., 1999. A discontinuous hp finite element method for convection-diffusion problems. Computer Methods in Applied Mechanics and Engineering 175, 311–341. URL: https://www.sciencedirect.com/science/article/pii/S0045782598003594, doi:10.1016/S0045-7825(98)00359-4.

[12] Bear, J., Cheng, A.H.D., 2010. Modeling Groundwater Flow and Contaminant Transport. volume 23. Springer Dordrecht. URL: http://link.springer.com/10.1007/978-1-4020-6682-5, doi:10.1007/978-1-4020-6682-5.

[13] Buès, M.A., Oltean, C., 2000. Numerical simulations for saltwater intrusion by the mixed hybrid finite element method and discontinuous finite element method. Transport in Porous Media 40, 171–200. URL: http://link.springer.com/article/10.1023/A%3A1006626230029, doi:10.1023/A:1006626230029.

[14] Cockburn, B., Karniadakis, G.E., Shu, C.W., 2000. The Development of Discontinuous Galerkin Methods. Springer. URL: http://link.springer.com/10.1007/978-3-642-59721-3_1, doi:10.1007/978-3-642-59721-3_1.

[15] Croucher, A.E., O'Sullivan, M.J., 1995. The Henry Problem for Saltwater Intrusion. Water Resources Research 31, 1809–1814. URL: http://doi.wiley.com/10.1029/95WR00431, doi:10.1029/95WR00431.

[16] Dawson, C., Sun, S., Wheeler, M.F., 2004. Compatible algorithms for coupled flow and transport. Computer Methods in Applied Mechanics and Engineering 193, 2565–2580. doi:10.1016/j.cma.2003.12.059.

[17] De Maet, T., Hanert, E., Vanclooster, M., 2014. A fully-explicit discontinuous Galerkin hydrodynamic model for variably-saturated porous media. Journal of Hydrodynamics 26, 594–607. URL: http://link.springer.com/10.1016/S1001-6058(14)60067-6, doi:10.1016/S1001-6058(14)60067-6.

[18] Di Pietro, D.A., Ern, A., 2011. Mathematical Aspects of Discontinuous Galerkin Methods. volume 3. Springer-Verlag Berlin Heidelberg. URL: http://books.google.com/books?id=ak-qQvWGA5oC&pgis=1, doi:10.1007/978-3-642-22980-0.

[19] Diersch, H.J., 1988. Finite element modelling of recirculating density-driven saltwater intrusion processes in groundwater. Advances in Water Resources 11, 25–43. URL: http://www.sciencedirect.com/science/article/pii/030917088890019X, doi:10.1016/0309-1708(88)90019-X.

[20] Diersch, H.J., Kolditz, O., 2002. Variable-density flow and transport in porous media: approaches and challenges. Advances in Water Resources 25, 899–944. URL: http://www.sciencedirect.com/science/article/pii/S0309170802000635, doi:10.1016/S0309-1708(02)00063-5.

[21] Diersch, H.J.G., 2014. FEFLOW: Finite element modeling of flow, mass and heat transport in porous and fractured media. volume 9783642387. 1 ed., Springer. doi:10.1007/978-3-642-38739-5.

[22] Dolejší, V., Kuraz, M., Solin, P., 2019. Adaptive higher-order space-time discontinuous Galerkin method for the computer simulation of variably-saturated porous media flows. Applied Mathematical Modelling 72, 276–305. URL: https://www.sciencedirect.com/science/article/pii/S0307904X19301222?via%3Dihub, doi:10.1016/j.apm.2019.02.037.

[23] Epshteyn, Y., Rivière, B., 2006. On the solution of incompressible two-phase flow by a p-version discontinuous Galerkin method, in: Communications in Numerical Methods in Engineering, pp. 741–751. doi:10.1002/cnm.846.

[24] Epshteyn, Y., Rivière, B., 2007. Fully implicit discontinuous finite element methods for two-phase flow. Applied Numerical Mathematics 57, 383–401. URL: http://www.sciencedirect.com/science/article/pii/S0168927406000912, doi:10.1016/j.apnum.2006.04.004.

[25] Epshteyn, Y., Rivière, B., 2008. Convergence of high order methods for miscible displacement. International Journal of Numerical Analysis and Modeling 5, 47–63.

[26] Ern, A., Mozolevski, I., Schuh, L., 2010. Discontinuous Galerkin approximation of two-phase flows in heterogeneous porous media with discontinuous capillary pressures. Computer Methods in Applied Mechanics and Engineering 199, 1491–1501. URL: http://www.sciencedirect.com/science/article/pii/S0045782509004204, doi:10.1016/j.cma.2009.12.014.

[27] Fabien, M.S., Knepley, M.G., Rivière, B.M., 2018. A hybridizable discontinuous Galerkin method for two-phase flow in heterogeneous porous media. International Journal for Numerical Methods in Engineering 116, 161–177. URL: http://doi.wiley.com/10.1002/nme.5919, doi:10.1002/nme.5919.

[28] Fahs, M., Ataie-Ashtiani, B., Younes, A., Simmons, C.T., Ackerer, P., 2016. The Henry problem: New semianalytical solution for velocity-dependent dispersion. Water Resources Research 52, 7382–7407. URL: http://doi.wiley.com/10.1002/2016WR019288, doi:10.1002/2016WR019288.

[29] Fahs, M., Younes, A., Makradi, A., 2015. A reference benchmark solution for free convection in a square cavity filled with a heterogeneous porous medium. Numerical Heat Transfer, Part B: Fundamentals 67, 437–462. URL: http://www.tandfonline.com/doi/abs/10.1080/10407790.2014.977183, doi:10.1080/10407790.2014.977183.

[30] Fahs, M., Younes, A., Mara, T.A., 2014. A new benchmark semi-analytical solution for density-driven flow in porous media. Advances in Water Resources 70, 24–35. URL: http://www.sciencedirect.com/science/article/pii/S0309170814000803, doi:10.1016/j.advwatres.2014.04.013.

[31] Franciolini, M., Fidkowski, K.J., Crivellini, A., 2020. Efficient discontinuous Galerkin implementations and preconditioners for implicit unsteady compressible flow simulations. Computers and Fluids 203, 104542. doi:10.1016/j.compfluid.2020.104542, arXiv:1812.04789.

[32] Frolkovič, P., 1998. Consistent velocity approximation for density driven flow and transport, in: In: Van Keer R et al., editors. Advanced computational methods in engineering, Part 2. Maastrich: Shaker Publishing, pp. 603–11.

[33] Frolkovič, P., De Schepper, H., 2001. Numerical modelling of convection dominated transport coupled with density driven flow in porous media. Advances in Water Resources 24, 63–72. URL: http://www.sciencedirect.com/science/article/pii/S0309170800000257, doi:10.1016/S0309-1708(00)00025-7.

[34] Fučík, R., Mikyška, J., 2011. Discontinous Galerkin and mixed-hybrid finite element approach to two-phase flow in heterogeneous porous media with different capillary pressures, in: Procedia Computer Science, Elsevier. pp. 908–917. URL: https://www.sciencedirect.com/science/article/pii/S1877050911001542, doi:10.1016/j.procs.2011.04.096.

[35] Goswami, R.R., Clement, T.P., 2007. Laboratory-scale investigation of saltwater intrusion dynamics. Water Resources Research 43, 1–11. URL: https://agupubs.onlinelibrary.wiley.com/doi/full/10.1029/2006WR005151, doi:10.1029/2006WR005151.

[36] Guevara Morel, C.R., van Reeuwijk, M., Graf, T., 2015. Systematic investigation of non-Boussinesq effects in variable-density groundwater flow simulations. Journal of contaminant hydrology 183, 82–98. URL: http://www.sciencedirect.com/science/article/pii/S0169772215300358, doi:10.1016/j.jconhyd.2015.10.004.

[37] Guo, W., Langevin, C.D., 2002. User's Guide to SEAWAT: A computer program for simulation of three-dimensional variable-density ground-water flow. Technical Report Book 6. U.S. Geological Survey.

[38] Hamidi, M., Sabbagh-Yazdi, S.R.R., 2008. Modeling of 2D density-dependent flow and transport in porous media using finite volume method. Computers Fluids 37, 1047–1055. URL: http://www.sciencedirect.com/science/article/pii/S0045793007001934, doi:10.1016/j.compfluid.2007.10.009.

[39] Henry, H.R., 1964. Effects of dispersion on salt encroachment in coastal aquifers: sea water in coastal aquifers. US Geological Survey Water Supply Paper , 70–84.

[40] Herbert, A.W., Jackson, C.P., Lever, D.A., 1988. Coupled groundwater flow and solute transport with fluid density strongly dependent upon concentration. Water Resources Research 24, 1781–1795. URL: http://doi.wiley.com/10.1029/WR024i010p01781, doi:10.1029/WR024i010p01781.

[41] Hirthe, E.M., Graf, T., 2012. Non-iterative adaptive time-stepping scheme with temporal truncation error control for simulating variable-density flow. Advances in Water Resources 49, 46–55. URL: https://www.sciencedirect.com/science/article/abs/pii/S0309170812002096, doi:10.1016/j.advwatres.2012.07.021.

[42] Hoteit, H., Firoozabadi, A., 2008a. An efficient numerical model for incompressible two-phase flow in fractured media. Advances in Water Resources 31, 891–905. URL: https://www.sciencedirect.com/science/article/abs/pii/S0309170808000353?via%3Dihub, doi:10.1016/j.advwatres.2008.02.004.

[43] Hoteit, H., Firoozabadi, A., 2008b. Numerical modeling of two-phase flow in heterogeneous permeable media with different capillarity pressures. Advances in Water Resources 31, 56–73. URL: https://www.sciencedirect.com/science/article/abs/pii/S030917080700108X?via%3Dihub, doi:10.1016/j.advwatres.2007.06.006.

[44] Hoteit, H., Firoozabadi, A., 2018. Modeling of multicomponent diffusions and natural convection in unfractured and fractured media by discontinuous Galerkin and mixed methods. International Journal for Numerical Methods in Engineering 114, 535–556. URL: http://doi.wiley.com/10.1002/nme.5753, doi:10.1002/nme.5753.

[45] Huyakorn, P.S., Andersen, P.F., Mercer, J.W., White H.O., J., White, H.O., 1987. Saltwater intrusion in aquifers: Development and testing of a three-dimensional finite element model. Water Resources Research 23, 293–312. URL: http://doi.wiley.com/10.1029/WR023i002p00293, doi:10.1029/WR023i002p00293.

[46] Jamei, M., Raeisi Isa-Abadi, A., Ahmadianfar, I., 2019. A Lax–Wendroff-IMPES scheme for a two-phase flow in porous media using interior penalty discontinuous Galerkin method. Numerical Heat Transfer, Part B: Fundamentals 75, 325–346. URL: https://www.tandfonline.com/doi/full/10.1080/10407790.2019.1627825, doi:10.1080/10407790.2019.1627825.

[47] Johannsen, K., 2003. On the Validity of the Boussinesq Approximation for the Elder Problem. Computational Geosciences 7, 169–182. URL: http://link.springer.com/article/10.1023/A%3A1025515229807, doi:10.1023/A:1025515229807.

[48] Klieber, W., Rivière, B., 2006. Adaptive simulations of two-phase flow by discontinuous Galerkin methods. Computer Methods in Applied Mechanics and Engineering 196, 404–419. URL: http://www.sciencedirect.com/science/article/pii/S0045782506001769, doi:10.1016/j.cma.2006.05.007.

[49] Kolditz, O., Ratke, R., Diersch, H.J.G.H.J., Zielke, W., 1998. Coupled groundwater flow and transport: 1. Verification of variable density flow and transport models. Advances in Water Resources 21, 27–46. URL: http://www.sciencedirect.com/science/article/pii/S0309170896000346, doi:10.1016/S0309-1708(96)00034-6.

[50] Kou, J., Sun, S., 2014. Upwind discontinuous Galerkin methods with mass conservation of both phases for incompressible two-phase flow in porous media. Numerical Methods for Partial Differential Equations 30, 1674–1699. URL: http://doi.wiley.com/10.1002/num.21817, doi:10.1002/num.21817.

[51] Kummer, F., 2017. Extended discontinuous Galerkin methods for two-phase flows: the spatial discretization. International Journal for Numerical Methods in Engineering 109, 259–289. URL: http://doi.wiley.com/10.1002/nme.5288, doi:10.1002/nme.5288.

[52] Li, H., Farthing, M.W., Dawson, C.N., Miller, C.T., 2007a. Local discontinuous Galerkin approximations to Richards' equation. Advances in Water Resources 30, 555–575. URL: https://www.sciencedirect.com/science/article/pii/S0309170806000662, doi:10.1016/j.advwatres.2006.04.011.

[53] Li, H., Farthing, M.W., Miller, C.T., 2007b. Adaptive local discontinuous Galerkin approximation to Richards' equation. Advances in Water Resources 30, 1883–1901. URL: https://www.sciencedirect.com/science/article/abs/pii/S0309170807000371?via%3Dihub, doi:10.1016/j.advwatres.2007.02.007.

[54] Li, J., Riviere, B., 2015a. High order discontinuous Galerkin method for simulating miscible flooding in porous media. Computational Geosciences 19, 1251–1268. URL: http://link.springer.com/10.1007/s10596-015-9541-4, doi:10.1007/s10596-015-9541-4.

[55] Li, J., Riviere, B., 2015b. Numerical solutions of the incompressible miscible displacement equations in heterogeneous media. Computer Methods in Applied Mechanics and Engineering 292, 107–121. URL: http://www.sciencedirect.com/science/article/pii/S0045782514004186, doi:10.1016/j.cma.2014.10.048.

[56] Mazzia, A., Putti, M., 2002. Mixed-finite element and finite volume discretization for heavy brine simulations in groundwater. Journal of Computational and Applied Mathematics 147, 191–213. URL: https://www.sciencedirect.com/science/article/pii/S0377042702004338, doi:10.1016/S0377-0427(02)00433-8.

[57] Miller, C.T., Dawson, C.N., Farthing, M.W., Hou, T.Y., Huang, J., Kees, C.E., Kelley, C.T., Langtangen, H.P., 2013. Numerical simulation of water resources problems: Models, methods, and trends. Advances in Water Resources 51, 405–437. URL: https://www.sciencedirect.com/science/article/pii/S0309170812001431, doi:10.1016/j.advwatres.2012.05.008.

[58] Moortgat, J., 2017. Adaptive implicit finite element methods for multicomponent compressible flow in heterogeneous and fractured porous media. Water Resources Research 53, 73–92. URL: http://doi.wiley.com/10.1002/2016WR019644, doi:10.1002/2016WR019644.

[59] Moortgat, J., Amooie, M.A., Soltanian, M.R., 2016. Implicit finite volume and discontinuous Galerkin methods for multicomponent flow in unstructured 3D fractured porous media. Advances in Water Resources 96, 389–404. doi:10.1016/j.advwatres.2016.08.007.

[60] Mozolevski, I., Schuh, L., 2013. Numerical simulation of two-phase immiscible incompressible flows in heterogeneous porous media with capillary barriers. Journal of Computational and Applied Mathematics 242, 12–27. URL: https://www.sciencedirect.com/science/article/pii/S0377042712004189, doi:10.1016/j.cam.2012.09.045.

[61] Oden, J.T., Babuška, I., Baumann, C.E., 1998. A discontinuous hp finite element method for diffusion problems. Journal of Computational Physics 146, 491–519.

[62] Oltean, C., Buès, M.A., 2001. Coupled Groundwater Flow and Transport in Porous Media. A Conservative or Non-conservative Form? Transport in Porous Media 44, 219–246. URL: https://link.springer.com/article/10.1023%2FA%3A1010778224076, doi:10.1023/A:1010778224076.

[63] Oude Essink, G., 1998. MOC3D adapted to simulate 3D density-dependent groundwater flow, in: Proceedings of the MODFLOW'98 Conference, Golden, Colorado, USA. pp. 291–303. URL: http://dspace.library.uu.nl/handle/1874/308773.

[64] Pinder, G.F., Cooper, H.H., 1970. A Numerical Technique for Calculating the Transient Position of the Saltwater Front. Water Resources Research 6, 875–882. URL: http://doi.wiley.com/10.1029/WR006i003p00875, doi:10.1029/WR006i003p00875.

[65] Prasad, A., Simmons, C.T., 2005. Using quantitative indicators to evaluate results from variable-density groundwater flow models. Hydrogeology Journal 13, 905–914. URL: http://link.springer.com/10.1007/s10040-004-0338-0, doi:10.1007/s10040-004-0338-0.

[66] Putti, M., Paniconi, C., 1995. Picard and Newton linearization for the coupled model for saltwater intrusion in aquifers. Advances in Water Resources 18, 159–170. URL: http://www.sciencedirect.com/science/article/pii/0309170895000065, doi:10.1016/0309-1708(95)00006-5.

[67] Raeisi Isa-Abadi, A., 2016. Modeling of seawater intrusion into heterogeneous coastal aquifers using discontinuous Galerkin method (in Persian). Phd thesis. Shahid Chamran University, Ahvaz, Iran.

[68] Rivière, B., 2008. Discontinuous Galerkin Methods for Solving Elliptic and Parabolic Equations. Society for Industrial and Applied Mathematics (SIAM), Philadelphia. URL: http://epubs.siam.org/doi/book/10.1137/1.9780898717440, doi:10.1137/1.9780898717440.

[69] Rivière, B., Wheeler, M.F., 2002. Discontinuous Galerkin methods for flow and transport problems in porous media. Communications in Numerical Methods in Engineering 18, 63–68. URL: http://doi.wiley.com/10.1002/cnm.464, doi:10.1002/cnm.464.

[70] Rivière, B., Wheeler, M.F., Girault, V., 1999. Improved energy estimates for interior penalty, constrained and discontinuous Galerkin methods for elliptic problems. Part I. Computational Geosciences 3, 337–360. URL: http://link.springer.com/article/10.1023/A%3A1011591328604, doi:10.1023/A:1011591328604.

[71] Segol, G., 1994. No Title. Classic Groundwater Simulations: Proving and Improving Numerical Models .

[72] Segol, G., Pinder, G.F., Gray, W.G., 1975. A Galerkin-finite element technique for calculating the transient position of the saltwater front. Water Resources Research 11, 343–347. URL: http://doi.wiley.com/10.1029/WR011i002p00343, doi:10.1029/WR011i002p00343.

[73] Shao, Q., Fahs, M., Hoteit, H., Carrera, J., Ackerer, P., Younes, A., 2018. A 3-D Semianalytical Solution for Density-Driven Flow in Porous Media. Water Resources Research 54, 10,094–10,116. URL: https://onlinelibrary.wiley.com/doi/abs/10.1029/2018WR023583, doi:10.1029/2018WR023583.

[74] Simmons, C.T., 2005. Variable density groundwater flow: From current challenges to future possibilities. Hydrogeology Journal 13, 116–119. URL: http://link.springer.com/10.1007/s10040-004-0408-3, doi:10.1007/s10040-004-0408-3.

[75] Simpson, M.J., Clement, T.P., 2003. Theoretical analysis of the worthiness of Henry and Elder problems as benchmarks of density-dependent groundwater flow models. Advances in Water Resources 26,

17–31. URL: http://www.sciencedirect.com/science/article/pii/S0309170802000854, doi:10.1016/S0309-1708(02)00085-4.

[76] Simpson, M.J., Clement, T.P., 2004. Improving the worthiness of the Henry problem as a benchmark for density-dependent groundwater flow models. Water Resources Research 40, 1–11. URL: http://doi.wiley.com/10.1029/2003WR002199, doi:10.1029/2003WR002199.

[77] Stoeckl, L., Walther, M., Graf, T., 2016. A new numerical benchmark of a freshwater lens. Water Resources Research 52, 2474–2489. URL: http://doi.wiley.com/10.1002/2015WR017989, doi:10.1002/2015WR017989.

[78] Sun, S., Rivière, B., Wheeler, M.F., 2002. A Combined Mixed Finite Element and Discontinuous Galerkin Method for Miscible Displacement Problem in Porous Media, in: Chan, T.F., Huang, Y., Tang, T., Xu, J., Ying, L.A. (Eds.), Recent Progress in Computational and Applied PDES. Springer US, Boston, MA, pp. 323–351. URL: http://www.springerlink.com/index/10.1007/978-1-4615-0113-8, doi:10.1007/978-1-4615-0113-8.

[79] Sun, S., Wheeler, M.F., 2005a. Discontinuous Galerkin methods for coupled flow and reactive transport problems. Applied Numerical Mathematics 52, 273–298. URL: https://www.sciencedirect.com/science/article/pii/S0168927404001710?via%3Dihub, doi:10.1016/j.apnum.2004.08.035.

[80] Sun, S., Wheeler, M.F., 2005b. Symmetric and Nonsymmetric Discontinuous Galerkin Methods for Reactive Transport in Porous Media. SIAM Journal on Numerical Analysis 43, 195–219. URL: http://epubs.siam.org/doi/abs/10.1137/S003614290241708X, doi:10.1137/S003614290241708X.

[81] Sun, S., Wheeler, M.F., 2006a. A posteriori error estimation and dynamic adaptivity for symmetric discontinuous Galerkin approximations of reactive transport problems. Computer Methods in Applied Mechanics and Engineering 195, 632–652. URL: http://www.sciencedirect.com/science/article/pii/S0045782505001222, doi:10.1016/j.cma.2005.02.021.

[82] Sun, S., Wheeler, M.F., 2006b. Analysis of Discontinuous Galerkin Methods for Multicomponent Reactive Transport Problems. Computers and Mathematics with Applications 52, 637–650. URL: https://www.sciencedirect.com/science/article/pii/S0898122106002458?via%3Dihub, doi:10.1016/j.camwa.2006.10.004.

[83] Sun, S., Wheeler, M.F., 2006c. Anisotropic and dynamic mesh adaptation for discontinuous Galerkin methods applied to reactive transport. Computer Methods in Applied Mechanics and Engineering 195, 3382–3405. URL: https://www.sciencedirect.com/science/article/pii/S0045782505002744?via%3Dihub, doi:10.1016/j.cma.2005.06.019.

[84] Voss, C.I., Simmons, C.T., Robinson, N.I., 2010. Three-dimensional benchmark for variable-density flow and transport simulation: matching semi-analytic stability modes for steady unstable convection

in an inclined porous box. Hydrogeology Journal 18, 5–23. URL: http://link.springer.com/10.1007/s10040-009-0556-6, doi:10.1007/s10040-009-0556-6.

[85] Voss, C.I., Souza, W.R., 1987. Variable density flow and solute transport simulation of regional aquifers containing a narrow freshwater-saltwater transition zone. Water Resources Research 23, 1851–1866. URL: http://doi.wiley.com/10.1029/WR023i010p01851, doi:10.1029/WR023i010p01851.

[86] Werner, A.D., Bakker, M., Post, V.E., Vandenbohede, A., Lu, C., Ataie-Ashtiani, B., Simmons, C.T., Barry, D., 2013. Seawater intrusion processes, investigation and management: Recent advances and future challenges. Advances in Water Resources 51, 3–26. URL: http://linkinghub.elsevier.com/retrieve/pii/S030917081200053X, doi:10.1016/j.advwatres.2012.03.004.

[87] Wheeler, M.F., Sun, S., Eslinger, O., Rivière, B., 2003. Discontinuous Galerkin Method for Modeling Flow and Reactive Transport in Porous Media, in: Wendland, W., Efendiev, M. (Eds.), Analysis and Simulation of Multifield Problems, Lecture Notes in Applied and Computational Mechanics. Springer Berlin Heidelberg, Berlin, Heidelberg. volume 12 of *Lecture Notes in Applied and Computational Mechanics*, pp. 37–56. URL: http://link.springer.com/10.1007/978-3-540-36527-3_3, doi:10.1007/978-3-540-36527-3.

[88] Younes, A., Ackerer, P., 2008. Solving the advection-dispersion equation with discontinuous Galerkin and multipoint flux approximation methods on unstructured meshes. International Journal for Numerical Methods in Fluids 58, 687–708. URL: http://doi.wiley.com/10.1002/fld.1783, doi:10.1002/fld.1783.

[89] Younes, A., Ackerer, P., 2010. Empirical versus time stepping with embedded error control for density-driven flow in porous media. Water Resources Research 46, 1–8. URL: http://doi.wiley.com/10.1029/2009WR008229, doi:10.1029/2009WR008229.

[90] Younes, A., Fahs, M., 2013. A Semi-Analytical Solution for the Reactive Henry Saltwater Intrusion Problem. Water, Air, Soil Pollution 224, 1779. URL: http://link.springer.com/10.1007/s11270-013-1779-7, doi:10.1007/s11270-013-1779-7.

[91] Younes, A., Fahs, M., 2014. A semi-analytical solution for saltwater intrusion with a very narrow transition zone. Hydrogeology Journal 22, 501–506. URL: http://link.springer.com/10.1007/s10040-014-1102-8, doi:10.1007/s10040-014-1102-8.

[92] Younes, A., Fahs, M., Ahmed, S., 2009. Solving density driven flow problems with efficient spatial discretizations and higher-order time integration methods. Advances in Water Resources 32, 340–352. URL: http://www.sciencedirect.com/science/article/pii/S0309170808002133, doi:10.1016/j.advwatres.2008.11.003.

[93] Zidane, A., Firoozabadi, A., 2014. An efficient numerical model for multicomponent compressible flow in fractured porous media. Advances in Water Resources 74, 127–147. doi:10.1016/j.advwatres.2014.08.010.

[94] Zidane, A., Firoozabadi, A., 2015. An implicit numerical model for multicomponent compressible two-phase flow in porous media. Advances in Water Resources 85, 64–78. doi:10.1016/j.advwatres.2015.09.006.

[95] Zidane, A., Younes, A., Huggenberger, P., Zechner, E., 2012. The Henry semianalytical solution for saltwater intrusion with reduced dispersion. Water Resources Research 48, 1–10. URL: http://www.agu.org/pubs/crossref/2012/2011WR011157.shtml, doi:10.1029/2011WR011157.